1 Title: **Erasable Hippocampal Neural Signatures Predict Memory Discrimination**

2 Authors: *Kinsky, Nathaniel R.[1,3,5], Orlin, Daniel J.[3,4,5], Ruesch, Evan A.[3], Kim, Brian[1,2], Coello,
3 Siria[3], Diba, Kamran[1,2], *Ramirez, Steve[3]

4 Summary

5 Memories involving the hippocampus can take several days to consolidate, challenging efforts
6 to uncover the neuronal signatures underlying this process. Using calcium imaging in freely
7 moving mice, we tracked the hippocampal dynamics underlying memory formation across a ten-
8 day contextual fear conditioning (CFC) task. Following learning, context-specific place field
9 remapping correlated with memory performance. To causally test whether these hippocampal
10 dynamics support memory consolidation, we induced amnesia in a group of mice by
11 pharmacologically blocking protein synthesis immediately following learning. We found that
12 halting protein synthesis following learning paradoxically accelerated cell turnover and also
13 arrested learning-related remapping, paralleling the absence of remapping observed in
14 untreated mice that exhibited poor memory expression. Finally, coordinated neural activity that
15 emerged following learning was dependent on intact protein synthesis and predicted memory-
16 related freezing behavior. We conclude that context-specific place field remapping and the
17 development of coordinated ensemble activity require protein synthesis and underlie contextual
18 fear memory consolidation.

19 Introduction

20 The process of memory consolidation requires protein synthesis following learning to produce
21 stable long-term memories (Barondes & Cohen, 1968; Davis & Squire, 1984; Squire &
22 Barondes, 1974). At the synaptic level, protein synthesis is necessary for the formation of late-
23 phase but not early-phase long-term potentiation (LTP) in hippocampal (HPC) neurons (Frey &
24 Morris, 1997; Huang et al., 1994; Nguyen et al., 1994). At the behavioral level, blocking protein
25 synthesis following learning impairs long-term memory for hippocampus-dependent contextual
26 fear conditioning (CFC) while leaving short term memory intact (Ryan et al., 2015; Schafe et al.,
27 1999). These studies suggest that memory consolidation requires new proteins to reinforce
28 learning-related connections which are potentiated during learning. Despite the evidence linking
29 *in vitro* synaptic potentiation to memory consolidation, little is known about how protein
30 synthesis *in vivo* influences the functional coding properties of neurons before, during, and after
31 learning to support memory consolidation. Experience-dependent remapping of place fields in
32 the hippocampus, which requires NMDA receptor dependent-plasticity (Dupret et al., 2010), is
33 thought to reflect learning-related reorganization of the hippocampal network (Bostock et al.,

[1]Department of Anesthesiology, University of Michigan Medical School, Ann Arbor, MI 48109, USA
[2]Neuroscience Graduate Program, University of Michigan, Ann Arbor, MI 48109, USA
[3]Center for Systems Neuroscience, Boston University, Boston, MA 02451, USA
[4]Neuroscience Graduate Program, Oregon Health & Science University, Portland, OR 97239, USA
[5]These authors contributed equally to this work
*Corresponding authors. Correspondence should be addressed to N.R.K (nkinsky@umich.edu) or S.R. (dvsteve@bu.edu)

34   1991; Colgin et al., 2008). Therefore, to causally test the hypothesis that lasting, learning-
35   related place-cell remapping (Muller & Kubie, 1987) is necessary for consolidation of a CFC
36   memory (Moita et al., 2004; Wang et al., 2012) we combined *in vivo* calcium imaging in mice
37   with systemic administration of the protein synthesis inhibitor, anisomycin, and tracked the
38   evolution, remapping, and stabilization of HPC place fields during and after CFC. Finally, we
39   leveraged the ability to record from large cell ensembles to investigate whether blocking protein
40   synthesis disrupted the development of coordinated neural activity predictive of freezing
41   behavior. Our results indicate that context-specific remapping and coordinated, freeze-
42   predicting ensemble activity emerge in a protein-synthesis dependent manner following learning
43   to support CFC memory consolidation.

44   Results

45   **Hippocampal neural dynamics between arenas predicts memory specificity**

46   Weeks prior to training, all mice received viral infusions of the genetically encoded calcium
47   indicator GCaMP6f (Chen et al., 2013) in region CA1 of the dorsal hippocampus. Subsequently,
48   following two days of pre-exposure ("Before" learning, days -2 and -1) to an open field (neutral
49   arena) and an operant chamber (shock arena) mice received a mild foot-shock on day 0
50   (training), after which they were moved to their home cage and immediately given systemic
51   injections of either anisomycin (ANI group) or vehicle (CTRL group). The shock arena recording
52   immediately followed each neutral arena recording, separated by approximate 5 minutes to
53   disconnect the recording camera and move the mouse the other room/arena. We then
54   performed a test of short-term memory 4 hours later and three tests of long-term memory 1, 2,
55   and 7 days following training (Figure 1A), each time by measuring freezing behavior. We titrated
56   the shock level during training such that the mice froze significantly more in the shock arena
57   relative to the neutral arena following learning while still exploring the majority of both arenas.
58   Nonetheless, we observed a range of freezing levels during the day 1 and 2 memory tests
59   (Figure S1A) and subsequently sub-divided CTRL mice into two groups: Learners, who froze
60   significantly more in the shock arena, and Non-Learners, who either showed generalized
61   freezing or froze at low levels in both arenas (Figures 1B and Figure S1B,E). Learners exhibited
62   reduced freezing on day 7, indicative of extinction (Figure 1B). All subsequent analyses related
63   to long-term memory therefore utilized the day 1 and 2 recall sessions ("After" learning and
64   consolidation). In contrast, mice in the ANI group exhibited no difference in freezing between
65   arenas at any time point, indicating that blocking protein synthesis impaired context-specific fear
66   memory (Figure 1C). To assess memory specificity, we calculated a behavioral discrimination
67   index (DI_{beh}) which quantified how much each animal froze in the shock vs. neutral arenas.
68   Negative DI values indicated higher freezing in the shock arena. Learners exhibited negative
69   DI_{beh} levels on days 1 and 2 that were significantly different from both Non-Learners (by
70   definition) and from the ANI group as well (Figure 1D). Variability in freezing on the days prior to
71   shock could indicate heightened anxiety by some mice, which could in turn influence contextual
72   fear learning. However, we found no difference between groups in thigmotaxis, a metric of
73   anxiety (Figure S1F-G). Both the CTRL and ANI groups exhibited significant freezing in the
74   shock arena during the 4 hour test, though we note that the behavior in the ANI group at this
75   time point could arise from either contextual fear or non-specific aversive effects of anisomycin
76   treatment (Figure S2) since these mice froze at high levels in both arenas.

77   We visualized the activity of pyramidal neurons in region CA1 of the dorsal hippocampus
78   (Figure 1E) using a miniaturized epifluorescence microscope (Ghosh et al., 2011; Ziv et al.,

79 2013). We identified a large number of neurons in each 10 minute session (n = 128 to 1216,
80 Figure S3), extracted their corresponding calcium traces (Figure 1F), and tracked them between
81 sessions throughout the CFC task, which allowed us to determine the long-term evolution of the
82 HPC neural code. We noticed that many neurons exhibited strong changes in mean event rate
83 between arenas (Figure 1F) and calculated a neural discrimination index (DI_{neural}) to quantify the
84 distinctiveness of neural activity between arenas (0 = similar, 1 = distinct). Same-day neural
85 discrimination between arenas correlated strongly with across-day neural discrimination in the
86 same arena (Figure S1D). This indicates that mice exhibit natural variability in neural
87 discrimination which is invariant between different arenas and across time.

88
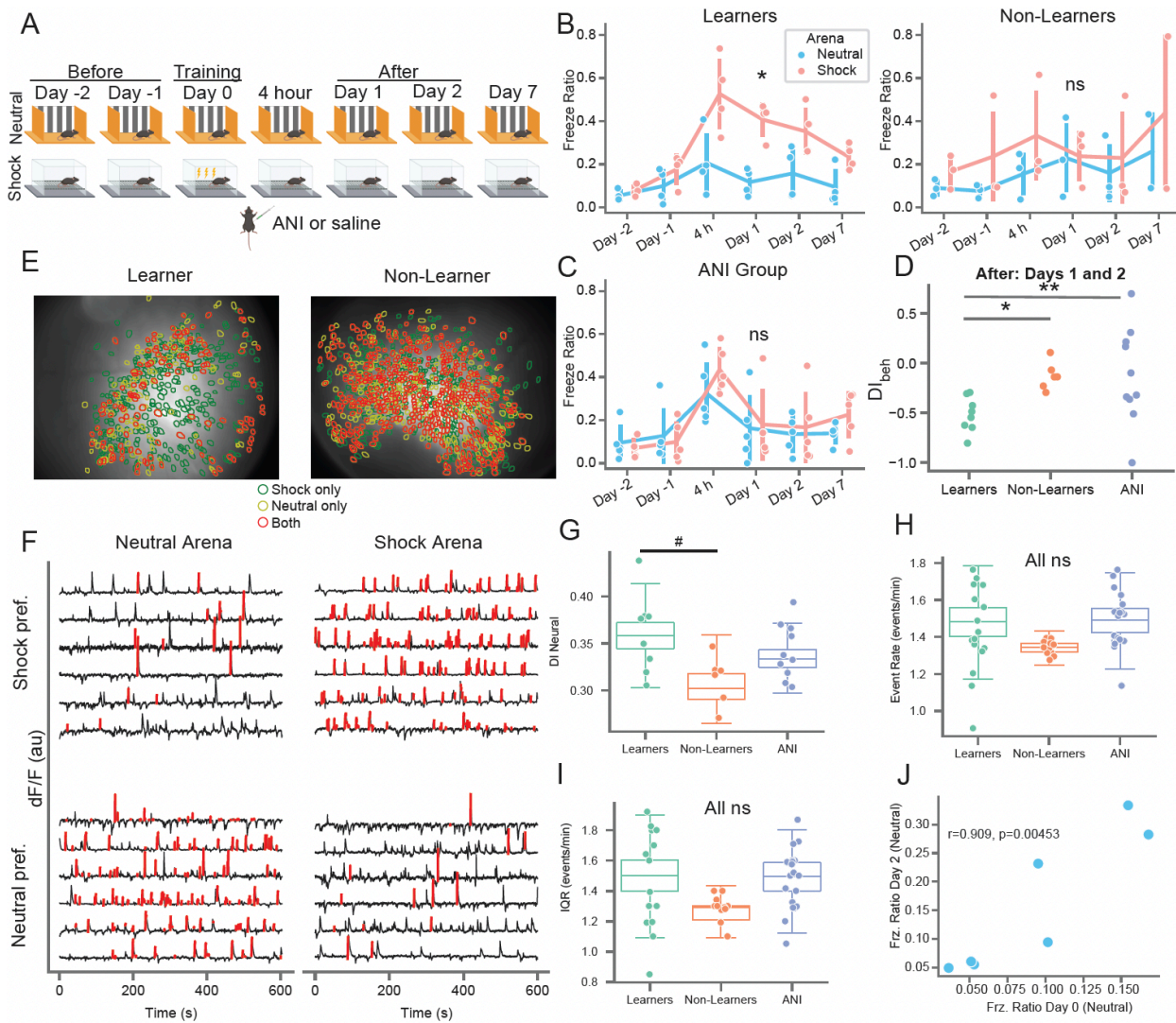
90 **Figure 1: Mice exhibit variability in memory recall and neural activity prior to learning in a protein-synthesis dependent contextual**
91 **fear conditioning task. A)** Schematic of the behavioral paradigm. Mice freely explored two distinct arenas (neutral and shock) for 10
92 minutes each day. Mice underwent mild contextual fear conditioning on day 0 in the shock arena followed by immediate I.P. administration of
93 anisomycin or vehicle in their home cage. Memory recall tests were conducted 4 hours and 1, 2, and 7 days post-shock. The time of each
94 session is referenced to the shock session. **B)** (left) Learner (CTRL) mice freezing on all days. Red = shock arena, blue = neutral arena.
95 *p=4.5e-0.4 shock – neutral freezing from day-1 to day 1 one-sided paired t-test (n=4 mice, t=13.4). (right) Same but for Non-Learner (CTRL)
96 mice (n=3 mice, p=0.249, t=0.819). **C)** Same as B but for ANI group (n=5 mice, p=0.219, t=0.859). **D)** Behavioral discrimination between
97 arenas after shock (Days 1-2) shows formation of a specific fear memory for Learners only, by definition (positive = more freezing in neutral
98 arena, negative = more freezing in shock arena, 0 = equal freezing in both arenas). *p= 3.78e-4(t=4.48), **p=0.0229 (t=2.17) 1-sided t-test of
99 mean DI value from Days 1 & 2, n=8/6/10 sessions for Learners/Non-Learners/ANI group, **E)** (left) Neural overlap plots between neutral and

3

100 shock arenas for an example Learner mouse on day -1, before shock. Green = cells active in the shock arena only, yellow = cells active in
101 the neutral arena only, orange = cells active in both arenas. (right) Same for example Non-Learner on day -2 showing higher overlap of
102 active cells between arenas. **F)** Example calcium activity from the Learner mouse shown in C (left) for cells active in both arenas. Black =
103 calcium trace, red = putative spiking activity during transient rises. Top row shows shock arena preferring cells, bottom row shows neutral
104 arena preferring cells. **G)** Neural discrimination index (DIneural) between groups on Days -2 and -1. Boxplots show population median and
105 1st/3rd quartiles (whiskers, 95% CI) estimated using hierarchical bootstrapping (HB) data with session means overlaid in dots, #p=0.09 after
106 Bonferroni correction for multiple comparisons. **H)** Same as G) but for event rate in Shock arena, **I)** Same as G) but for event rate
107 interquartile range (IQR) in Shock arena. **J)** Freezing in Neutral arena on Day 2 vs. Neutral arena on Day 0. Pearson correlation value and p-
108 value (two-sided) shown on plot. Statistics for G-J: un-paired one-sided HB test for days -2 and -1 after Bonferroni correction, n=10,000
109 bootstraps.

110 Surprisingly, we noticed that Learners exhibited a trend toward higher DI$_{neural}$ values compared
111 to Non-Learners in the sessions prior to the shock that did not reach significance (Figure 1G).
112 This was not due to higher activity rates for Non-Learners since we found no differences
113 between groups in mean event rate and or distribution of event rates on the days prior to shock
114 (Figure 1H-I). Finally, we found that freezing behavior the day of training correlated with Neutral
115 arena freezing during the 4 Hour and Day 2 recall sessions and exhibited a trend toward
116 correlation on Days 1 and 7 (Figure 1J and Figure S1H). These results indicate that the animal's
117 behavioral state the day of conditioning, and potentially neural discrimination between arenas
118 prior to learning, can influence memory specificity.

Blocking protein synthesis disrupts persistent neural activity following learning and arrests learning-related place field remapping

121 Next, we probed how arresting protein synthesis impacted HPC dynamics. Previous studies by
122 us and others have found that hippocampal cells exhibit constant turnover over time such that
123 the subset of active cells slowly changes over time (Kinsky et al., 2018; Ziv et al., 2013). We
124 hypothesized that, by preventing plasticity, ANI administration would slow or stop the normal
125 rate of cell turnover, measured as the overlap of active cells at each timepoint with the first day
126 recording day (Figure 2A). Surprisingly, ANI administration temporarily accelerated cell turnover
127 between the Day -1 and 4 hour session after which turnover rate returned to normal (Figure 2B,
128 C). We noticed that the normalized number of active neurons also appeared to be lower for the
129 ANI group compared to the CTRL group at the 4 hour session when anisomycin was still on
130 board, and potentially the following sessions, which could contribute to increased turnover
131 (Figure 2D). However, diminished cell activity could also result from reduced locomotion (Rich et
132 al., 2014), which we observed in both groups following conditioning / anisomycin. To
133 disentangle the effects of anisomycin and locomotion, we therefore fit the normalized number of
134 cells observed in each recording session to a generalized linear model with arena, freezing
135 ratio, anisomycin status (acute = 4 hr session, after = Day 1, 2, and 7), experimental group, and
136 anisomycin status x experimental group as covariates (Methods). Under this framework, we
137 found a highly significant influence of freezing ratio on active cell number ($p=2.3 \times 10^{-5}$) and a
138 trend toward fewer active cells for the ANI group at the 4 hour session (p=0.056) and following
139 sessions (p=0.094) that did not reach significance (Figure 2D). These results indicate that
140 reduced locomotion is the primary driver of reduced cell activity observed following anisomycin
141 administration. To test whether reduced activity resulted from cell death, we injected a separate
142 cohort of mice with either saline or anisomycin and then performed immunohistochemistry to
143 stain for apoptosis 4 hours after injection. We found negligible levels of apoptosis overall with no
144 difference between groups (Figure S4). We also observed no difference in the mean height of
145 calcium transients (a measure of signal-to-noise ratio) for neurons active before, during, or after
146 ANI administration, indicating that the observed decrease in the number of active neurons was
147 not due to differences in Ca2+ levels or depletion of the GCaMP protein (Figure S5D-E). To
148 confirm that anisomycin administration did not suppress network activities, which was reported

4

149 for intracranial infusions (but not systemic injections) of protein synthesis inhibitors in
150 anesthetized or immobile rodents (Barondes & Cohen, 1966; Sharma et al., 2012: Park et al.,
151 2023), we performed extracellular recordings in freely moving rats implanted with a linear probe
152 in the CA1 region of the hippocampus following administration of anisomycin. We observed
153 preserved theta activity, theta modulation of spiking, and robust sharp wave ripple activity for up
154 to 5 hours following anisomycin administration (Figure S5A-C). These observations indicate that
155 blocking protein synthesis following learning does not simply abolish all neuronal activity but
156 instead acutely accelerates the turnover of cells which may be specifically involved in learning.
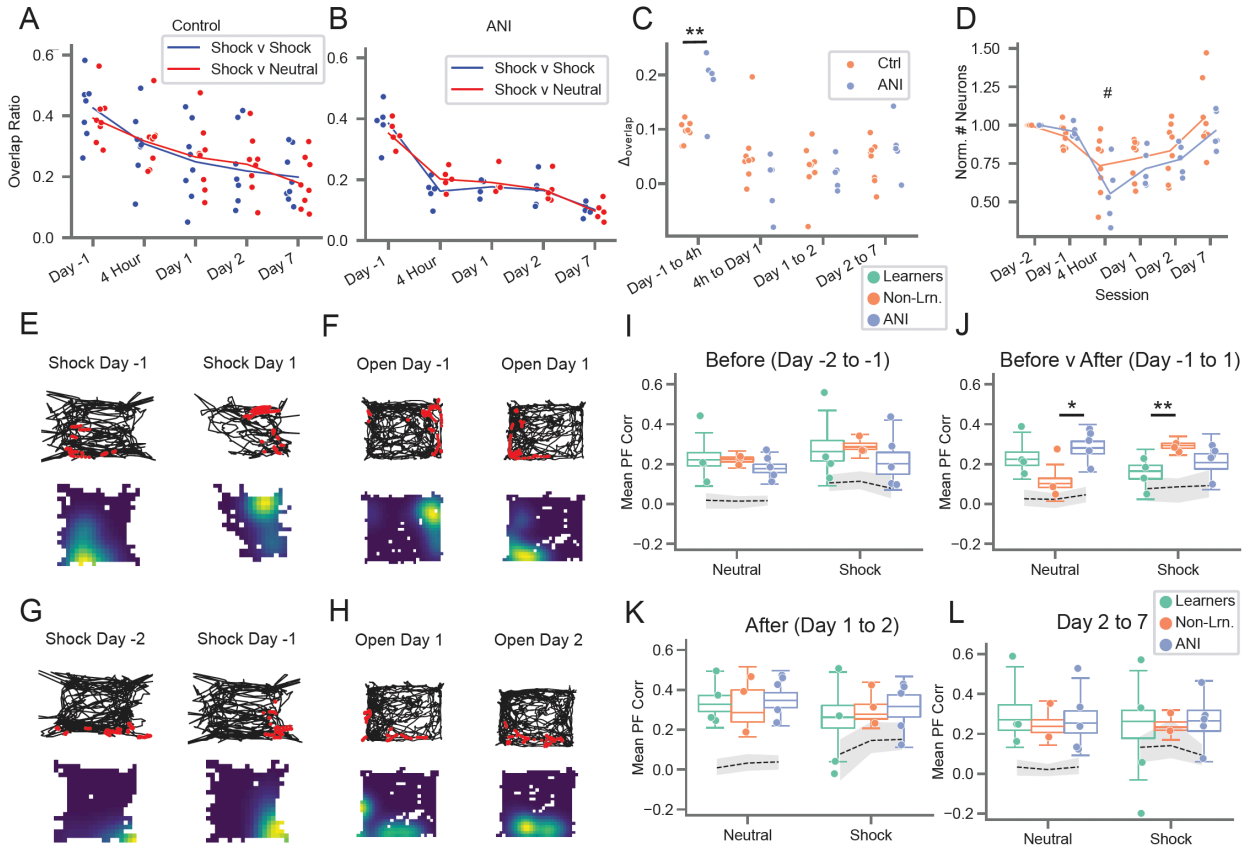
157

Figure 2: Preventing protein synthesis accelerates cell turnover and stifles learning-related place field remapping. A) Cell
overlap ratio with Day -2 session, CTRL group. Blue = within shock arena, red = shock v. neutral arena. **B)** Same as A) but for ANI
group. **C)** Change in overlap ratios from A) and B), dots show values from both arenas for each mouse, **p=0.00174 two-sided t-test
of mean value for each mouse (t=4.11, n=7 Ctrl mice and 5 ANI mice). **D)** Number of active neurons observed each day, normalized
to day -1. p=2.e-5 freeze-ratio, #p=0.056 group x 4 hr session interaction, p=0.094 group x after interaction, generalized linear
model. **E)** and **F)** Example place fields exhibiting learning-related remapping. **E)** Place field in shock arena from Learner mouse.
(*top*) Example mouse trajectory (black) with calcium activity (red) overlaid for the same cell from day -2 to -1 in shock arena,
(*bottom*) occupancy normalized rate maps for the same cells with warm colors indicating areas of high calcium activity. **F)** Same as
E) but for Non-Learner mouse in Neutral arena. **G)** and **H)** Example stable place fields. **G)** Same as E) but for a different cell from
same mouse in the shock arena prior to conditioning. **H)** Same as F) but for a different cell from the same mouse in the neutral
arena after conditioning. **I)** Place field correlations for all mice before shock (Days -2 and -1), boxplots show population median and
1st/3rd quartiles (whiskers, 95% CI) estimated using hierarchical bootstrapping (HB) data with session means overlaid in dots.
Dashed line and grey shading show mean and 95% CI of correlations calculated from shuffling cell identify 1000 times between
sessions. **J)** Same as I) but for Day -1 to Day 1, *p=0.0496, **p=0.0034. **K)** Same as I) but for Day 1 to Day 2. **L)** Same as I) but for
Day 2 to Day 7. Statistics for I-L: un-paired one-sided HB test after Bonferroni correction, n=10,000 bootstraps.

173 We next hypothesized that arresting protein synthesis, which disrupts the permanence of newly
174 formed place fields (Agnihotri et al., 2004), would likewise impair the long-term stability of CFC-
175 related remapping (Moita et al., 2004; Wang et al., 2012). We therefore assessed place field

5

176 remapping within and across epochs by correlating event rate maps for all neurons active
177 between two sessions (Figure 2E-L) following administration of anisomycin, compared with
178 saline. We noticed that place fields recorded in the Learners group exhibited very low across-
179 session correlations in the neutral arena throughout the experiment (Figure S6), which could
180 indicate remapping. However, in a separate study, we observed what appeared to be
181 remapping between two recording sessions, but which was actually a coherent rotation of all
182 place fields around a singular point (Kinsky et al., 2018), indicative of confusion in an animal's
183 axis of orientation, such as between west and north (Keinath et al., 2017). Importantly, such
184 angular disorientation does not impair the ability of mice to identify specific places (Julian et al.,
185 2015), and between-cell firing relationships are maintained during coherent rotations whereas
186 they are scrambled following remapping. Coherent rotations match the geometry of the
187 environment, e.g. producing rotations in 60 degree increments in a triangle versus 90 degrees in
188 square environments such as our neutral and shock arenas. Therefore, to ensure we were not
189 mistaking coherent rotations for remapping, we rotated all place field maps from each session in
190 90 degree increments and used only the orientation that produced the highest correlation
191 between sessions.

192 We found generally higher correlations compared to using non-rotated maps (Figure 2I-L vs.
193 Figure S6F), confirming that coherent rotations occurred in many recording sessions. In
194 particular, place field correlations were high both before learning and after consolidation for all
195 groups (Figure 2I, K, L and Figure S7), though Learner correlations trended toward lower
196 stability after shock (Figure 2K, L) which could indicate extinction (Wang et al., 2015). We then
197 compared place fields between session to assess short-term (Figure S8, 4 hour session to Days
198 -1 and 1) and long-term (Figure 2J, Day -1 to Day 1) learning-related remapping. In agreement
199 with previous studies (Moita et al., 2004; Wang et al., 2012), Learner place fields remapped
200 from Day -1 to Day 1, as indicated by lower correlations in the shock arena compared to the
201 other groups (Figure 2J, Figure S7B). Interestingly, Non-Learners exhibited lower place map
202 correlations from Day -1 to Day 1 in the neutral arena compared to the other groups, indicating
203 paradoxically stable place fields in the shock arena but remapping in the neutral arena (Figure
204 2J, Figure S7C, Figure S8C). We observed similar results when examining population vector
205 correlations (Figure S9). If learning causes remapping, this double dissociation indicates that
206 Non-Learner memory deficits might result from improperly associating the neutral arena with
207 shock. In contrast, the place maps of mice in the ANI group displayed high correlations in both
208 arenas across all time points, including after learning (Figure 2I-L, Figure S7E-F). This deficit in
209 remapping following anisomycin therefore indicates that protein synthesis is required to stabilize
210 the set of place fields which emerge following learning to support memory consolidation.
211 Overall, these observations indicate that remapping is necessary for the creation of context-
212 specific memories and that a lack of remapping, or improperly remapping, may underlie the
213 memory deficits observed in Non-Learners and in the ANI group.

Coordinated freeze-predictive neural activity emerges following consolidation

215 In addition to the spatial code, hippocampal neural activity can also reflect non-spatial variables
216 in a task (McKenzie et al., 2014; Muzzio et al., 2009; Wood et al., 1999). We noticed that, in line
217 with recent studies (Lee & Han, 2022; Schuette et al., 2020), many hippocampal neurons
218 reliably produced calcium transients around the time that mice froze (Figure 3A-B, D-F and
219 S10A-C). We observed similar proportions of peri-freeze tuned cells across all groups and
220 recording sessions, even before CFC (Figure S10D-E). Examining the +/- 4 seconds around

221   freezing events for Days 1-2 (after learning) revealed that population-level neural activity
222   peaked in the 2 seconds prior to freezing for control mice compared to the ANI group (Figure
223   3C) but did not differ between Learners and Non-Learners (Figure S10F). This pre-freeze
224   increase in activity for the CTRL vs. the ANI group was not present before learning or at the 4
225   hour session (Figure S10L-M). After learning, neurons with significant peri-freeze tuning tiled the
226   entire +/- 4 seconds around freeze onset (Figure 3G). However, the average peak timing of cells
227   with significant peri-freeze activity shift shifted to significantly early time points for Learners vs.
228   Non-Learners and ANI mice after learning (Figure 3H) with ~70% of cells active before freeze
229   onset. We therefore refer to these neurons as freeze-predictive cells, noting that the predictive
230   nature of their activity is pronounced in Learners compared to Non-Learners and the ANI group.

231   To quantify the reliability of freeze-predictive turning within cells, we tracked the peak, peri-
232   freeze calcium event probability of each freeze cell backwards and forwards in time from the
233   Day 1 recall session, after putative memory consolidation had occurred. We found that freeze-
234   predictive cells exhibited much higher tuning stability spanning from the 4 hour recall to the day
235   1 recall sessions in Learners than did these cells in other groups (Figure 3I). This indicates that
236   in Learners, reliable freeze-predictive tuning began to emerge between 4 hours and 1 day
237   following learning and was maintained thereafter (see Figure 3E for exemplar cell). In contrast,
238   peri-freezing activities in mice from the ANI group and in Non-Learners were more transient and
239   unreliable during this time span.

240   Next, we investigated whether the higher reliability of freeze-predicting cells in Learners was
241   related to increased co-activity (see Figure 3A-B) in this neuronal subpopulation by calculating
242   pairwise coactivation of neurons +/- 4 seconds from freeze onset. We found that pairwise
243   coactivation increased significantly from 0-2 seconds prior to freezing during the 4 hour and Day
244   1-2 sessions for Learners but not for Non-Learners or for ANI group mice (Figure 3J-L). We
245   observed a similar, but much less pronounced, increase for Learners in the Neutral arena for
246   the after learning recall session (Figure 3M). To account for the overall increase in population-
247   level activity prior to freezing (Figure 3C), we calculated chance level pairwise coactivation by
248   shuffling the order of freeze onsets for one cell in each pair 1000 times and determined the
249   probability that the actual pairwise chance exceeded shuffle for each bin. We found that the
250   proportion of freeze-predicting cells with significant coactivation (> 3 consecutive bins with
251   coactivity exceeding 95% of shuffles) increased for Learners, but not Non-Learners or ANI
252   group mice, from before learning to the 4 hour recall session and before learning to after
253   learning recall sessions (Figure 3N).

254   We then examined whether we observed similar increases in co-activity in the overall neural
255   population. To quantify this, we calculated the covariance between all cell pairs. We found that
256   the covariance of all cell-pairs increased significantly following CFC for Learners for both the 4
257   hour and after recall sessions (Figure S10H). Furthermore, the observed covariance increase
258   was not driven by freeze-predictive activity (Figure S10J). We observed a similar increase in
259   covariance for the ANI group at the 4hr session and a much smaller, but significant, increase
260   during the after recall sessions (Figure S10H). We observed no such increase for the ANI group
261   when we excluded freezing times from the covariance calculation (Figure S10I). These
262   increases were not observed prior to shock in the neutral arena (Figure S10G), suggesting that
263   the heightened covariance we observed was related to CFC learning. Consistent with our
264   pairwise coactivity analyses, we found a trend toward increase covariance of freeze-predicting
265   cells during the after recall sessions for Learners, but not Non-Learners or ANI mice (Figure

7

266   3O). We observed a similar trend in freeze-predicting cell covariance when we downsampled
267   the number of freezing events following learning to match that on days -2 and -1 (Figure S10I).
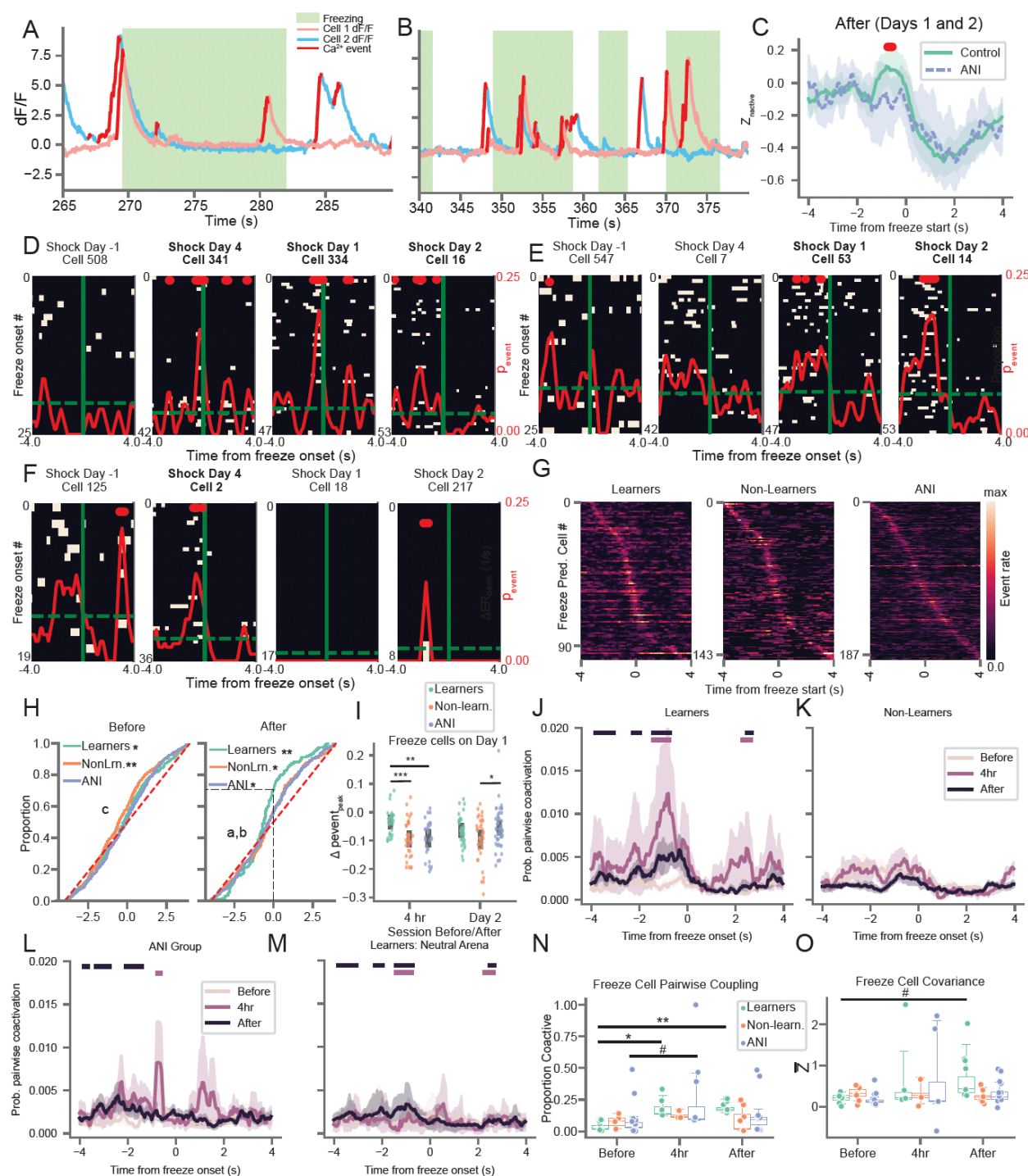
Figure 3: Arresting protein synthesis suppresses the development of coordinated freeze-predicting neural activity. **A) and B)** Example traces from two freeze-predicting cells which exhibit coordinated activity prior to freezing event during the day 1 memory recall session in the shock arena. Red = putative spiking activity, pink = cell shown in C, blue = cell shown in E. **C)** After learning (Days 1 and 2), z-scored population level calcium activity peaks between 0 and 2 seconds prior to freezing for CTRL relative to the ANI group. Line/shading = mean +/- 95% CI. Red: bins with p < 0.05, independent t-test (one-sided, n=7 CTRL mice and 5 ANI mice). **D) and E)** Example Learner freeze-predicting cells identified during the 4 hour (D) or day 1 (E) memory test tracked across

275 sessions. Peri-event calcium activity rasters are centered on freeze onset time (solid green). Dashed green = baseline calcium
276 event probability, red solid = peri-freeze calcium event probability, bins with p<0.01 (circular permutation test, n=1000) noted with
277 red bars at top. D/E corresponds to pink/blue cells shown in A-B. Bold = session with significant freeze-tuning. **F)** Same as D and E
278 but for ANI mouse freeze-predicting cell identified during the 4 hour session. **G)** Peri-freeze calcium event probability for all freeze-
279 predicting cells detected for each group after learning (Days 1-2), sorted by time of peak activation. **H)** (left) Cumulative distribution
280 of peak peri-freeze activation times before learning. *p=0.49, **p=1e-5 two-sided Wilcoxon rank-sum test , c: p=0.005 Non-Learners
281 v. ANI, 1-sided Mann-Whitney U-test (n = 329/458/543 neurons for Learners/Non-Learners/ANI group) (right) same as left but for
282 after learning. *p < 0.022, **p=2e-7 two-sided Wilcoxon rank-sum test. a: p=0.022 Learners v. Non-Learners, b: p=0.029 Learners v.
283 ANI 1-sided Mann-Whitney U-test (n=194/315/366 neurons for Learners/Non-Learners/ANI group). **I)** Change in peak peri-freeze
284 calcium event probability for all freeze-predicting cells detected during the Day 1 session and either the 4 hour or Day 2 session. p <
285 0.02 1-way ANOVA each day separately, *p=0.02, **p=0.001, ***p=0.0006 post-hoc Mann-Whiney U-test (n=30/35/29 4h to Day 1
286 cells and n = 35/37/45 Day 1 to Day 2 cells for Learners/Non-Learners/ANI group. **J)** Pairwise coactivation probability of all freeze-
287 predicting cells for Learners during Before, 4 hour, and After sessions in Shock arena. Maroon/Black bars at top indicate significant
288 increases in coactivation at 4 hour / After time points compared to before, p< 0.05 1-sided Mann-Whitney U-test (n= 4). **K)** Same as
289 J) but for Non-Learners (n=3). **L)** Same as K) but for ANI group (n= 5). **M)** Same as K) but for Learners in Neutral Arena (n=4). **N)**
290 Proportion of freeze-predictive cells with significant pairwise coactivation compared to chance (trial shuffle). *p=4e-8, **p=3.6e-7,
291 #p=0.093. boxplots show population median and 1st/3rd quartiles (whiskers, 95% CI) estimated using hierarchical bootstrapping (HB)
292 data with session means overlaid in dots. **O)** Freeze-predicting cells exhibit a trend toward increased peri-freeze covariance (z-
293 scored relative to the Day -2 and -1 covariance values for all cells) for Learners but not Non-Learners or ANI group mice. Mean
294 covariance of freeze-predictive cells from each session shown. #p=0.06. Statistics for K and O: un-paired one-sided HB test after
295 Bonferroni correction, n=10,000 shuffles.

296   Finally, we performed additional analyzes focused on the same set of freeze-predictive cells
297   conditioned on their activity during the Day 1 recall test immediately after putative memory
298   consolidation was finalized. Freeze-predicting cells identified on the 1 day recall session
299   displayed a trend toward increased covariance following CFC in Learners but not in Non-
300   Learners or in the ANI group (Figure S10K). However, these cells did not exhibit increased
301   covariance during the previous day's 4 hour session, suggesting that even though freeze-
302   predictive activity begins to emerge immediately following learning, functional cell connections
303   continue to reorganize up to one day later to form coordinated ensembles. These results
304   demonstrate that freeze-predictive tuning emerges following learning and continues to take
305   shape in the ensuing hours until it stabilizes one day later. Importantly, the coordination of these
306   freeze-predictive cells into neuronal ensembles requires protein synthesis, and they fail to
307   coactivate under memory consolidation failures.

308   <u>Discussion</u>

309   The results of our study provide evidence that HPC spatial and non-spatial representations
310   support contextual memory formation and consolidation. We first probed how protein-synthesis
311   influenced learning-related hippocampal dynamics following CFC. We saw that anisomycin
312   acutely accelerate cell turnover in the 4 hours following learning. In addition to this turnover
313   acceleration, anisomycin's amnestic effects coincided with a reduction in learning-related
314   remapping, effectively halting HPC contextual representations in their prior state. This paralleled
315   the absence of remapping in the shock arena for Non-Learners, providing strong evidence for
316   the persistence of remapping as a mechanism underlying spatial memory consolidation. Given
317   that remapping *was* observed in Learners during this time window, we speculate that arresting
318   protein synthesis temporarily blocked the formation of new place-fields in the subset of cells that
319   would otherwise undergo remapping following CFC. By this conjecture, existing synapses were
320   weakened to enable the formation of new connections between cells, and these new
321   connections were stifled by anisomycin, diminishing the excitatory drive to these cells to the
322   point where calcium activity was no longer observable. This idea is resonant with the notion that
323   more excitable/active neurons are preferentially involved in memory trace formation (Rashid et
324   al., 2016; Sweis et al., 2021). It also provides an explanation for why we observed accelerated
325   cell turnover following ANI administration as the cells involved in learning are effectively

326 silenced, allowing for a new set of cells to become active. Reduced activity – which may arise
327 from non-specific effects of ANI, or the blockage of constitutive protein translation (Scavuzzo et
328 al., 2019) – could also underlie increased cell turnover. However, our study does not support
329 this view. Consistent with a recent paper which found that ANI did not silence hippocampal
330 neuron activity (Park et al., 2023), we did not observe a widespread shutdown of neural activity
331 as we found that both theta oscillations and sharp-wave ripples were intact in ANI-treated mice.

332 Surprisingly, remapping occurred in untreated mice that exhibited poor memory recall (Non-
333 Learners); however, this remapping was limited to the neutral arena. This indicates that ANI
334 induced memory failures and poor learning manifest via the same underlying mechanism – a
335 failure to remap in the shock arena – but with important differences. ANI impairs memory by
336 preventing learning-related plasticity which stifles remapping, while poor learning can occur
337 when the shock is improperly associated with the neutral arena, causing remapping therein. In
338 line with previous studies, we found that fear conditioning induced place field remapping in
339 Learners in the shock arena (Wang et al., 2012; Moita et al., 2004). Surprisingly, however, Non-
340 Learners also exhibited remapping, but in the neutral arena only. If remapping is a neural
341 substrate for spatial learning, we speculate that this might explain the increased freezing
342 behavior observed for Non-Learners in the neutral arena: they are improperly associating the
343 neutral arena with shock. Alternatively, the observed remapping could be an indicator of low
344 hippocampal engagement during the task, which has been shown to decrease discrimination
345 between two similar arenas (Wiltgen et al., 2010). However, under either of these situations, we
346 would also expect to observe remapping in the shock arena since Non-Learners freeze equally
347 in both contexts. Future studies could shed further light on this phenomenon. Overall, our
348 findings support the view that the long-term stability of learning-related remapping requires
349 protein synthesis and underlies CFC memory consolidation.

350 Memory generalization or linking occurs when mice freeze at high levels in a neutral arena. Cai
351 et al. (2016) demonstrated that exposing mice to two arenas five hours apart compared to
352 seven days apart increases the likelihood of memory linking. Despite the close temporal
353 proximity between arena exposures in this experiment, our intent was not to increase contextual
354 fear memory/generalization. Instead, our protocol was designed to produce a moderate level of
355 freezing following conditioning, specifically in the shock arena, as too much freezing would
356 cause insufficient exploration to observe place fields. While close temporal exposure between
357 the conditioning and neutral arena can increase the likelihood of memory linking, it does not
358 guarantee it. Many other factors, such as the amount of pre-exposure time (Frankland et al.,
359 2004) and familiarity with the general experimental procedure can influence contextual memory
360 generalization. It should also be noted that, even procedures designed specifically to create
361 linked/generalized memories produce large variability in freezing levels, with many mice
362 exhibiting low levels of memory linking despite a 5 hour separation between arena exposures
363 (Shen et al., 2022). In contrast, some mice can exhibit generalized freezing in a neutral arena
364 which they never seen before (Wiltgen et al., 2010). The observed variability in memory
365 linking/generalization we observed in our control mice therefore agrees with the high levels of
366 variability observed in previous studies.

367 Next, we found that a subset of hippocampal cells reliably activated near freezing events during
368 fear memory recall, consistent with previous reports (Schuette et al., 2020; Mocle et al., 2024).
369 These cells activities were particularly heightened 1-2 seconds prior to freezing epochs in
370 animals that exhibited a strong, specific CFC memory but not in the ANI group or untreated

10

371 mice that exhibited poor memory. The predictive nature of these cells distinguishes them from
372 previously reported immobility cells which occur primarily in CA2 but also in CA1 (Kay et al.,
373 2016). We further found that freeze-predictive cells organized into reliable, co-active neuronal
374 ensembles following learning (Lee & Han, 2022; Rajasethupathy et al., 2015). Importantly, the
375 covariance of all cells increased incrementally for both ANI and Learner groups at the 4 hour
376 recall session, a time point at which protein synthesis is not considered to be required for the
377 induction of (early-phase) long-term potentiation *in vitro* (Frey & Morris, 1997; Nguyen et al.,
378 1994)*. However, at later time points, when protein synthesis *is* required to maintain (late-phase)
379 long-term potentiation (Frey et al., 1993; Nguyen et al., 1994), between-cell covariance
380 remained high for Learners only, consistent with a recent study demonstrating that the strength
381 of correlated activity in ventral CA1 neurons responsive to a foot shock predicted the strength of
382 contextual fear memory retrieval (Jimenez et al., 2020). It is important to note that all Control
383 mice exhibited heightened calcium activity 1-2 seconds prior to freezing epochs; however,
384 freeze-predictive neurons exhibited higher stability and coactivity for Learners compared to Non-
385 Learners and ANI mice. Therefore, in addition to maintaining learning-related synaptic changes
386 over hours to days, protein synthesis might also be instrumental for producing coordinated firing
387 of large ensembles of neurons to support memory recall.

388 The synchronous bursts of neuron ensembles we observed prior to freezing may provide a
389 neuronal basis for memory recall. For example, they could indicate the activation of sharp-wave
390 ripples (SWRs): transient, high frequency oscillations observable in the hippocamp local field
391 potential which can facilitate transmitting information throughout the cortex. SWRs are primarily
392 observed during periods of awake immobility and sleep and are hypothesized support memory
393 consolidation and planning through reactivation of neuronal activity patterns observed during
394 learning and active exploration (Buzsáki, 2015). However, SWRs can also occur during periods
395 of movement; these exploratory SWRs (eSWRs) are posited to strengthen connections between
396 place cells for reactivation and subsequent stabilization during sleep (O'Neill et al., 2006). In line
397 with this view, synchronous neuronal activation during eSWRs could strengthen connections
398 between freeze-predicting cells and stabilize their activity patterns to guide future memory
399 recall. Alternatively, coordinated activation of these cells could cooccur with other prominent
400 hippocampal oscillations such as theta or gamma (Colgin, 2016). Whether it occurs with SWRs,
401 theta, or gamma, coincident firing of freeze-predictive ensembles could be important for guiding
402 memory recall. In line with this idea, one study demonstrated that synchronous optogenetic
403 stimulation of engram neurons tagged during learning could artificially reactivate a fear memory
404 even when normal long-term recall of the fear memory was hindered by arresting protein
405 synthesis after learning, suggesting that a memory trace still resided in the network (Ryan et al.,
406 2015). Our findings provide a parsimonious explanation for this previous result by demonstrating
407 that anisomycin halts the co-activation of freeze-predictive cells, weakening the capacity of
408 these neurons to transmit behavior-related information to downstream regions through
409 coincident firing (Lisman, 1997) and impairing their ability to trigger memory recall (Ryan &
410 Frankland, 2022).

411 Overall, our results provide a bridge between the neuronal activities that underly memory
412 formation and the protein signaling events that are critical for plastic modification of synapses,
413 indicating that protein synthesis is necessary for the formation of new stable spatial
414 representations of an aversive context following learning and for producing coordinated activity
415 of freeze-predictive neurons.

Limitations of the study

In this study, we casually test how post-learning protein synthesis impacts the neural dynamics related to contextual memory consolidation and recall in the hippocampus. We find that protein synthesis is required for place cells to remap following learning and for freeze-predicting neurons to develop lasting functional connections. We utilized systemic injections of anisomycin to pharmacologically arrest protein synthesis. While anisomycin has been used for decades to block memory consolidation and disrupt long-term potentiation, it produces many off target effects including malaise, which we show in Figure S2, and which could contribute to the accelerated cell turnover and lower cell activity observed in the ANI group following administration. Moreover, it lacks temporal, regional, and cell-type specificity. Therefore, we are unable to determine whether the pharmacologic memory consolidation failure we induce is due to blocking protein synthesis or due to other, non-specific effects, including an acceleration of cell turnover or due to disruptive effects in non-hippocampal brain regions. Future studies could utilize more specific approaches (Shrestha et al., 2020) to disentangle this question. Nonetheless, this study's finding that anisomycin blocks the coactivity of freeze-predictive cell-pairs is consistent with previous literature demonstrating that protein synthesis is required to produce lasting long-term potentiation between different groups of neurons (Frey and Morris, 1997). We also utilize systemic injections rather than local infusions of anisomycin due to location of a GRIN lens immediately over the hippocampus. The neural and behavioral effects of anisomycin could therefore be due to disruption of protein synthesis in other, non-hippocampal, regions. Regardless, our results are consistent with previous behavioral studies using local hippocampal infusions to block contextual fear memory consolidation and lesion studies demonstrating that the hippocampus is necessary for contextual fear memory formation and consolidation (Kim & Fanselow, 1992; Debiec et al., 2002; Rossatto et al., 2007; Ocampo et al., 2017). Last, we utilize calcium imaging to capture neural activity, which allows for tracking of individual neurons across all stages of the experiment. However, due to the slower temporal dynamics of GCaMP, we are unable to capture fast time-scale hippocampal activity, such as SWRs, reactivation, replay, and theta sequences, that are important for memory formation and consolidation. Future studies could use electrophysiology to explore how these phenomena are likewise impacted by protein synthesis.

463 Investigator Grant from the Brain and Behavior Research Foundation, a Ludwig Family
464 Foundation grant, and the McKnight Foundation Memory and Cognitive Disorders award, and
465 Boston University's Neurophotonics Center.

466 <u>Author Contributions</u>

467 Conceptualization: N.R.K with the help of Howard Eichenbaum; Methodolgy: N.R.K; Software:
468 N.R.K., E.A.R; Validation: N.R.K; Formal Analysis: N.R.K, D.J.O., E.A.R, B.K; Investigation:
469 N.R.K., D.J.O., E.A.R., B.K, S.C.; Data Curation: N.R.K., D.J.O., E.A.R., B.K.; Writing – original
470 draft preparation: N.R.K.; Writing – review and editing; N.R.K, D.J.O, E.A.R., B.K., K.D., S.R.;
471 Visualization: N.R.K.; Project Administration; N.R.K, S.R.; Funding Acquisition: N.R.K., K.D.,
472 S.R.

473 <u>Competing Interests</u>

474 The authors declare no competing interests.

475 <u>Materials & Correspondence</u>

476 All requests for materials and correspondence should be directed to Nat Kinsky
477 (nkinsky@umich.edu) or Steve Ramirez (dvsteve@bu.edu).

478 <u>References</u>

479 Agnihotri, N. T., Hawkins, R. D., Kandel, E. R., & Kentros, C. G. (2004). The long-term stability
480   of new hippocampal place fields requires new protein synthesis. *Proceedings of the*
481   *National Academy of Sciences*, *101*(10), 3656–3661.
482   https://doi.org/10.1073/pnas.0400385101

483 Barondes, S. H., & Cohen, H. D. (1966). Puromycin Effect on Successive Phases of Memory
484   Storage. *Science*, *151*(3710), 594–595. https://doi.org/10.1126/science.151.3710.594

485 Barondes, S. H., & Cohen, H. D. (1968). Memory impairment after subcutaneous injection of
486   acetoxycycloheximide. *Science (New York, N.Y.)*, *160*(3827), 556–557.
487   http://www.ncbi.nlm.nih.gov/pubmed/5689416

488 Bostock, E., Muller, R. U., & Kubie, J. L. (1991). Experience-dependent modifications of
489   hippocampal place cell firing. *Hippocampus*, *1*(2), 193–205.
490   https://doi.org/10.1002/hipo.450010207

491 Buzsáki, G. (2015). Hippocampal sharp wave-ripple: A cognitive biomarker for episodic memory
492   and planning. *Hippocampus*, *25*(10), 1073–1188. https://doi.org/10.1002/hipo.22488

493 Cai, D. J., Aharoni, D., Shuman, T., Shobe, J., Biane, J., Lou, J., Kim, I., Baumgaertel, K.,
494   Levenstain, A., Tuszynski, M., Mayford, M., & Silva, A. J. (2016). A shared neural
495   ensemble links distinct contextual memories encoded close in time. *Nature*, *534*, 115–118.
496   https://doi.org/10.1038/nature17955

497 Chen, T.-W., Wardill, T. J., Sun, Y., Pulver, S. R., Renninger, S. L., Baohan, A., Schreiter, E. R.,
498   Kerr, R. a, Orger, M. B., Jayaraman, V., Looger, L. L., Svoboda, K., & Kim, D. S. (2013).
499   Ultrasensitive fluorescent proteins for imaging neuronal activity. *Nature*, *499*(7458), 295–
500   300. https://doi.org/10.1038/nature12354

501   Colgin, L. L. (2016). Rhythms of the hippocampal network. *Nature Reviews Neuroscience*,
502   *17*(4), 239–249. https://doi.org/10.1038/nrn.2016.21

503   Colgin, L. L., Moser, E. I., & Moser, M.-B. (2008). Understanding memory through hippocampal
504   remapping. *Trends in Neurosciences*, *31*(9), 469–477.
505   https://doi.org/10.1016/j.tins.2008.06.008

506   Debiec, J., LeDoux, J. E., & Nader, K. (2002). Cellular and systems reconsolidation in the
507   hippocampus. *Neuron*, *36*(3), 527–538. http://www.ncbi.nlm.nih.gov/pubmed/12408854

508   Davis, H. P., & Squire, L. R. (1984). Protein synthesis and memory: A review. *Psychological*
509   *Bulletin*, *96*(3), 518–559. https://doi.org/10.1037/0033-2909.96.3.518

510   Dupret, D., O'Neill, J., Pleydell-Bouverie, B., & Csicsvari, J. (2010). The reorganization and
511   reactivation of hippocampal maps predict spatial memory performance. *Nature*
512   *Neuroscience*, *13*(8), 995–1002. https://doi.org/10.1038/nn.2599

513   Frey, U., Huang, Y.-Y., & Kandel, E. R. (1993). Effects of cAMP Simulate a Late Stage of LTP in
514   Hippocampal CA1 Neurons. *Science*, *260*(5114), 1661–1664.
515   https://doi.org/10.1126/science.8389057

516   Frey, U., & Morris, R. G. M. (1997). Synaptic tagging and long-term potentiation. *Nature*,
517   *385*(6616), 533–536. https://doi.org/10.1038/385533a0

518   Geva, N., Deitch, D., Rubin, A., & Ziv, Y. (2023). Time and experience differentially affect
519   distinct aspects of hippocampal representational drift. *Neuron*, *111*(15), 2357-2366.e5.
520   https://doi.org/10.1016/j.neuron.2023.05.005

521   Ghosh, K. K., Burns, L. D., Cocker, E. D., Nimmerjahn, A., Ziv, Y., Gamal, A. El, & Schnitzer, M.
522   J. (2011). Miniaturized integration of a fluorescence microscope. *Nature Methods*, *8*(10),
523   871–878. https://doi.org/10.1038/nmeth.1694

524   Huang, Y. Y., Li, X. C., & Kandel, E. R. (1994). cAMP contributes to mossy fiber LTP by
525   initiating both a covalently mediated early phase and macromolecular synthesis-dependent
526   late phase. *Cell*, *79*(1), 69–79. https://doi.org/10.1016/0092-8674(94)90401-4

527   Julian, J. B., Keinath, A. T., Muzzio, I. A., & Epstein, R. A. (2015). Place recognition and
528   heading retrieval are mediated by dissociable cognitive systems in mice. *Proceedings of*
529   *the National Academy of Sciences*, *112*(20), 6503–6508.
530   https://doi.org/10.1073/pnas.1424194112

531   Kay, K., Sosa, M., Chung, J., Karlsson, M. P., Larkin, M., Grossrubatscher, I., & Frank, L. M.
532   (2016). A hippocampal network for spatial coding during immobility. *Nature*, *531*, 185–190.
533   https://doi.org/10.1038/nature17144

534   Keinath, A. T., Julian, J. B., Epstein, R. A., & Muzzio, I. A. (2017). Environmental Geometry
535   Aligns the Hippocampal Map during Spatial Reorientation. *Current Biology*, *27*(3).
536   https://doi.org/http://dx.doi.org/10.1016/j.cub.2016.11.046

537   Kim, J. J., & Fanselow, M. S. (1992). Modality-specific retrograde amnesia of fear. *Science*,
538   *256*(5057), 675–677. http://www.ncbi.nlm.nih.gov/pubmed/1585183

539   Kinsky, N. R., Mau, W., Sullivan, D. W., Levy, S. J., Ruesch, E. A., & Hasselmo, M. E. (2020).
540   Trajectory-modulated hippocampal neurons persist throughout memory-guided navigation.
541   *Nature Communications*, 1–14. https://doi.org/10.1038/s41467-020-16226-4

542   Kinsky, N. R., Sullivan, D. W., Mau, W., Hasselmo, M. E., & Eichenbaum, H. B. (2018).
543   Hippocampal Place Fields Maintain a Coherent and Flexible Map across Long Timescales.
544   *Current Biology*, *28*(22), 1–11. https://doi.org/10.1016/J.CUB.2018.09.037

545   Kinsky, N. R., Vöröslakos, M., Lopez Ruiz, J. R., Watkins de Jong, L., Slager, N., McKenzie, S.,
546   Yoon, E., & Diba, K. (2023). Simultaneous electrophysiology and optogenetic perturbation
547   of the same neurons in chronically implanted animals using µLED silicon probes. *STAR*
548   *Protocols*, *4*(4). https://doi.org/10.1016/j.xpro.2023.102570

549   Lee, H.-S., & Han, J.-H. (2022). Activity patterns of individual neurons and ensembles correlated
550   with retrieval of a contextual memory in the dorsal CA1 of mouse hippocampus. *The*
551   *Journal of Neuroscience*, *43*(1), JN-RM-1407-22. https://doi.org/10.1523/jneurosci.1407-
552   22.2022

553   Levy, S. J., Kinsky, N. R., Mau, W., Sullivan, D. W., & Hasselmo, M. E. (2021). Hippocampal
554   spatial memory representations in mice are heterogeneously stable. *Hippocampus*, *31*(3),
555   244–260. https://doi.org/10.1002/hipo.23272

556   Lisman, J. E. (1997). Bursts as a unit of neural information: Making unreliable synapses reliable.
557   *Trends in Neurosciences*, *20*(1), 38–43. https://doi.org/10.1016/S0166-2236(96)10070-9

558   Mankin, E. A., Sparks, F. T., Slayyeh, B., Sutherland, R. J., Leutgeb, S., & Leutgeb, J. K.
559   (2012). Neuronal code for extended time in the hippocampus. *Proceedings of the National*
560   *Academy of Sciences*, *109*(47), 19462–19467. https://doi.org/10.1073/pnas.1214107109

561   Mau, W., Sullivan, D. W., Kinsky, N. R., Hasselmo, M. E., Howard, M. W., & Eichenbaum, H. B.
562   (2018). The Same Hippocampal CA1 Population Simultaneously Codes Temporal
563   Information over Multiple Timescales. *Current Biology*, *28*(10), 1499-1508.e4.
564   https://doi.org/10.1016/j.cub.2018.03.051

565   McKenzie, S., Frank, A. J., Kinsky, N. R., Porter, B., Rivière, P. D., & Eichenbaum, H. B. (2014).
566   Hippocampal representation of related and opposing memories develop within distinct,
567   hierarchically organized neural schemas. *Neuron*, *83*(1), 202–215.
568   https://doi.org/10.1016/j.neuron.2014.05.019

569   Mocle, A. J., Ramsaran, A. I., Jacob, A. D., Rashid, A. J., Luchetti, A., Tran, L. M., Richards, B.
570   A., Frankland, P. W., & Josselyn, S. A. (2024). Excitability mediates allocation of pre-
571   configured ensembles to a hippocampal engram supporting contextual conditioned threat
572   in mice. Neuron, 1–11. https://doi.org/10.1016/j.neuron.2024.02.007

573   Moita, M. A. P., Rosis, S., Zhou, Y., LeDoux, J. E., & Blair, H. T. (2004). Putting Fear in Its
574   Place: Remapping of Hippocampal Place Cells during Fear Conditioning. *Journal of*
575   *Neuroscience*, *24*(31), 7015–7023. https://doi.org/10.1523/JNEUROSCI.5492-03.2004

576   Muir, D. R., & Kampa, B. M. (2015). FocusStack and StimServer: a new open source MATLAB
577   toolchain for visual stimulation and analysis of two-photon calcium neuronal imaging data.
578   *Frontiers in Neuroinformatics*, *8*(January), 1–13. https://doi.org/10.3389/fninf.2014.00085

Muller, R. U., & Kubie, J. L. (1987). The effects of changes in the environment on the spatial firing of hippocampal complex-spike cells. *The Journal of Neuroscience*, *7*(7), 1951–1968. http://www.ncbi.nlm.nih.gov/pubmed/3612226

Muzzio, I. A., Levita, L., Kulkarni, J., Monaco, J. D., Kentros, C. G., Stead, M., Abbott, L. F., & Kandel, E. R. (2009). Attention enhances the retrieval and stability of visuospatial and olfactory representations in the dorsal hippocampus. *PLoS Biology*, *7*(6). https://doi.org/10.1371/journal.pbio.1000140

Nguyen, P., Abel, T., & Kandel, E. R. (1994). Requirement of a critical period of transcription for induction of a late phase of LTP. *Science*, *265*(5175), 1104–1107. https://doi.org/10.1126/science.8066450

Ocampo, A. C., Squire, L. R., & Clark, R. E. (2017). Hippocampal area CA1 and remote memory in rats. *Learning & Memory*, *24*, 563–569. https://doi.org/10.1101/lm.045781.117.24

Olypher, A. V, Lánský, P., Muller, R. U., & Fenton, A. A. (2003). Quantifying location-specific information in the discharge of rat hippocampal place cells. *Journal of Neuroscience Methods*, *127*(2), 123–135. https://doi.org/10.1016/S0165-0270(03)00123-7

O'Neill, J., Senior, T., & Csicsvari, J. (2006). Place-selective firing of CA1 pyramidal cells during sharp wave/ripple network patterns in exploratory behavior. *Neuron*, *49*(1), 143–155. https://doi.org/10.1016/j.neuron.2005.10.037

Park, E. H., Kao, H. Y., Jourdi, H., van Dijk, M. T., Carrillo-Segura, S., Tunnell, K. W., Gutierrez, J., Wallace, E. J., Troy-Regier, M., Radwan, B., Lesburguères, E., Alarcon, J. M., & Fenton, A. A. (2023). Phencyclidine Disrupts Neural Coordination and Cognitive Control by Dysregulating Translation. *Biological Psychiatry Global Open Science*, *4*(1), 252–263. https://doi.org/10.1016/j.bpsgos.2023.04.009

Rashid, A. J., Yan, C., Mercaldo, V., Hsiang, H. L., Park, S., Cole, C. J., Cristofaro, A. De, Yu, J., Ramakrishnan, C., Lee, S. Y., Deisseroth, K., Frankland, P. W., & Josselyn, S. A. (2016). Competition between engrams influences fear memory formation and recall. *Science*, *353*(6297), 383–388. https://doi.org/10.1126/science.aaf0594

Rajasethupathy, P., Sankaran, S., Marshel, J. H., Kim, C. K., Ferenczi, E., Lee, S. Y., Berndt, A., Ramakrishnan, C., Jaffe, A., Lo, M., Liston, C., & Deisseroth, K. (2015). Projections from neocortex mediate top-down control of memory retrieval. *Nature*, *526*(7575), 653–659. https://doi.org/10.1038/nature15389

Resendez, S. L., Jennings, J. H., Ung, R. L., Namboodiri, V. M. K., Zhou, Z. C., Otis, J. M., Nomura, H., McHenry, J. A., Kosyk, O., & Stuber, G. D. (2016). Visualization of cortical, subcortical and deep brain neural circuit dynamics during naturalistic mammalian behavior with head-mounted microscopes and chronically implanted lenses. *Nature Protocols*, *11*(3), 566–597. https://doi.org/10.1038/nprot.2016.021

Rossato, J. I., Bevilaqua, L. R. M., Myskiw, J. C., Medina, J. H., Izquierdo, I., & Cammarota, M. (2007). On the role of hippocampal protein synthesis in the consolidation and reconsolidation of object recognition memory. *Learning & Memory*, *14*(1–2), 36–46. https://doi.org/10.1101/lm.422607

620   Rubin, A., Geva, N., Sheintuch, L., & Ziv, Y. (2015). Hippocampal ensemble dynamics
621   timestamp events in long-term memory. *ELife*, *4*(December), 1–16.
622   https://doi.org/10.7554/eLife.12247

623   Ryan, T. J., & Frankland, P. W. (2022). Forgetting as a form of adaptive engram cell plasticity.
624   *Nature Reviews Neuroscience, 23*(3), 173–186. https://doi.org/10.1038/s41583-021-00548-
625   3

626   Ryan, T. J., Roy, D. S., Pignatelli, M., Arons, A., & Tonegawa, S. (2015). Engram cells retain
627   memory under retrograde amnesia. *Science*, *348*(6238), 1007–1013.
628   https://doi.org/10.1126/science.aaa5542

629   Saravanan, V., Berman, G. J., & Sober, S. J. (2020). Application of the hierarchical bootstrap to
630   multi-level data in neuroscience. *Neurons, Behavior, Data Analysis and Theory*, *3*(5), 1–25.
631   http://www.ncbi.nlm.nih.gov/pubmed/33644783%0Ahttp://www.pubmedcentral.nih.gov/articl
632   erender.fcgi?artid=PMC7906290

633   Scavuzzo, C. J., LeBlancq, M. J., Nargang, F., Lemieux, H., Hamilton, T. J., & Dickson, C. T.
634   (2019). The amnestic agent anisomycin disrupts intrinsic membrane properties of
635   hippocampal neurons via a loss of cellular energetics. *Journal of Neurophysiology*, *122*(3),
636   1123–1135. https://doi.org/10.1152/jn.00370.2019

637   Schafe, G. E., Nadel, N. V., Sullivan, G. M., Harris, A., & LeDoux, J. E. (1999). Memory
638   consolidation for contextual and auditory fear conditioning is dependent on protein
639   synthesis, PKA, and MAP kinase. *Learning and Memory*, *6*(2), 97–110.
640   https://doi.org/10.1101/lm.6.2.97

641   Schuette, P. J., Reis, F. M. C. V., Maechler, P., Chakerian, M., Torossian, A., Blair, G. J., Wang,
642   W., Blair, H. T., Fanselow, M. S., Kao, J. C., & Adhikari, A. (2020). Long-term
643   characterization of hippocampal remapping during contextual fear acquisition and
644   extinction. *The Journal of Neuroscience*, *September*, JN-RM-1022-20.
645   https://doi.org/10.1523/jneurosci.1022-20.2020

646   Sharma, A. V., Nargang, F. E., & Dickson, C. T. (2012). Neurosilence: Profound Suppression of
647   Neural Activity following Intracerebral Administration of the Protein Synthesis Inhibitor
648   Anisomycin. *The Journal of Neuroscience*, *32*(7), 2377–2387.
649   https://doi.org/10.1523/JNEUROSCI.3543-11.2012

650   Shrestha, P., Ayata, P., Herrero-Vidal, P., Longo, F., Gastone, A., LeDoux, J. E., Heintz, N., &
651   Klann, E. (2020). Cell-type-specific drug-inducible protein synthesis inhibition demonstrates
652   that memory consolidation requires rapid neuronal translation. *Nature Neuroscience*, *23*(2),
653   281–292. https://doi.org/10.1038/s41593-019-0568-z

654   Squire, L. R., & Barondes, S. H. (1974). Anisomycin, like other inhibitors of cerebral protein
655   synthesis, impairs 'long-term' memory of a discrimination task. *Brain Research*, *66*(2), 301–
656   308. https://doi.org/10.1016/0006-8993(74)90148-6

657   Sweis, B. M., Mau, W., Rabinowitz, S., & Cai, D. J. (2021). Dynamic and heterogeneous neural
658   ensembles contribute to a memory engram. *Current Opinion in Neurobiology*, *67*, 199–206.
659   https://doi.org/10.1016/j.conb.2020.11.017

660   Vöröslakos, M., Petersen, P. C., Vöröslakos, B., & Buzsáki, G. (2021). Metal microdrive and
661   head cap system for silicon probe recovery in freely moving rodent. *ELife*, *10*(x), 1–21.
662   https://doi.org/10.7554/eLife.65859

663   Wang, M. E., Wann, E. G., Yuan, R. K., Ramos Álvarez, M. M., Stead, S. M., & Muzzio, I. A.
664   (2012). Long-term stabilization of place cell remapping produced by a fearful experience.
665   *The Journal of Neuroscience*, *32*(45), 15802–15814.
666   https://doi.org/10.1523/JNEUROSCI.0480-12.2012

667   Wang, M. E., Yuan, R. K., Keinath, A. T., Ramos Alvarez, M. M., & Muzzio, I. A. (2015).
668   Extinction of Learned Fear Induces Hippocampal Place Cell Remapping. *Journal of*
669   *Neuroscience*, *35*(24), 9122–9136. https://doi.org/10.1523/JNEUROSCI.4477-14.2015

670   Wood, E. R., Dudchenko, P. A., & Eichenbaum, H. B. (1999). The global record of memory in
671   hippocampal neuronal activity. *Nature*, *397*(6720), 613–616. https://doi.org/10.1038/17605

672   Yger, P., Spampinato, G. L. B., Esposito, E., Lefebvre, B., Deny, S., Gardella, C., Stimberg, M.,
673   Jetter, F., Zeck, G., Picaud, S., Duebel, J., & Marre, O. (2018). A spike sorting toolbox for
674   up to thousands of electrodes validated with ground truth recordings in vitro and in vivo.
675   *ELife*, *7*, 1–23. https://doi.org/10.7554/eLife.34518

676   Ziv, Y., Burns, L. D., Cocker, E. D., Hamel, E. O., Ghosh, K. K., Kitch, L. J., El Gamal, A., &
677   Schnitzer, M. J. (2013). Long-term dynamics of CA1 hippocampal place codes. *Nature*
678   *Neuroscience*, *16*(3), 264–266. https://doi.org/10.1038/nn.3329

679

680 # STAR★Methods

681 ## Key resources table

REAGENT or RESOURCE	SOURCE	IDENTIFIER
Other		
pAAV (AAV9).Syn.GCaMP6f.WPRE.SV40	Addgene	100837
1 µL syringe	Hamilton	65458-02
Micro Injection pump	WPI	UMP3 + Micro4 Controller
Microendoscope + Data Acquisition Box	Inscopix	V2
1028 ch Recording system	Intan	RHS2000
32 channel headstage	Intan	C3314
32 channel linear probe	NeuroNexus	A1x32-5mm-50-177
32 channel uLED probe	Neurolight	Chronic 32ch Optoelectrode
Recording cable	Intan	Standard SPI cable
Metal microdrive	3D Neuro	R2Drive
Plastic microdrive and rat protective crown	Vöröslakos et al. (2021)[3]	https://doi.org/10.5281/zenodo.8209229
Software		
Mosaic 1.2 Image Post-processing software	Inscopix	V1.2
nVista Recording software	Inscopix	nVista
OSC1lite Software	This paper	https://doi.org/10.5281/zenodo.8209373
RHX Recording Software	Intan	RHX
OpenEphys GUI	OpenEphys	GUI
MATLAB	The MathWorks	2019b
TENASPIS: Custom MATLAB code for cell identification and Ca2+ transient extraction	Mau et al. (2018)	https://github.com/SharpWave/TENASPIS (v4)
Custom MATLAB code for cell registration and data analysis	Kinsky et al. (2018)	https://github.com/nkinsky/ImageCamp
Custom Python code for Ca2+ data analysis	This paper	https://github.com/nkinsky/Eraser

• Python	Python.org	3.9.18
• Numpy	Numpy.org	1.26.3
• Matplotlib	Matplotlib.org	3.8.2
• Seaborn	Seaborn.pydata.org	0.13.2
• Pingouin	Pingouin-stats.org	0.5.4
Custom Python code for electrophysiological data analysis	Kinsky et al. (2024)	https://github.com/diba-lab/NeuroPy
• Python	Python.org	3.11.6
• Numpy	Numpy.org	1.24.4
• Matplotlib	Matplotlib.org	3.8.0
• Seaborn	Seaborn.pydata.org	0.13.0
• Pingouin	Pingouin-stats.org	0.5.3

682

Experimental model and study participant details

683

684 Sixteen (n = 10 controls, 6 anisomycin) male C57/BL6 mice (Jackson Laboratories), age 16 to
685 22 weeks during behavioral and imaging experiments and weighing 25-32g were used in this
686 study. Three mice were excluded after performing this study: one mouse after histology
687 revealed the GRIN lens implant and viral expression to be medial to the intended imaging, while
688 the other two were excluded due to unstable/overexpression of GCaMP that produced aberrant
689 calcium activity which emerged toward the end of the experiment. After exclusion of these mice,
690 we retained 8 mice in the control (CTRL) group and 5 mice in the anisomycin group (ANI) group.
691 Additionally, behavioral video tracking files for one CTRL mouse were corrupted during
692 recording during all neutral field recordings from day 0 on: this mouse was excluded from all
693 analyses which required using behavior in the neutral arena (e.g., place field correlations and
694 any analyses where the CTRL group was split into Learners and Non-Learners). Mice were
695 socially housed in a vivarium on a 12 hour light-dark cycle with 1-3 other mice prior to surgery
696 and were housed singly thereafter. Mice were given free access to food and water throughout
697 the study. All procedures were performed in compliance with the guidelines of the Boston
698 University Animal Care and Use Committee.

699 One male Long Evans rat, 10 months old and weighing 480g, and one female Long Evans rat, 5
700 months old and weighing 240g, were used for the electrophysiological recordings in this study.
701 Rats were socially housed in a vivarium on an adjusted 12 hour light-dark cycle (lights on at
702 noon, off at midnight) with 1-3 other rats prior to surgery and given free access to food and
703 water throughout the study. One week following recovery from the second surgery (see below),
704 and prior to performing the experiments shown in Figure S5, the second rat was water restricted
705 and performed a separate set of experiments in which she ran for water reward on a linear track
706 during which cells were focally inhibited via delivery of light from one of 12 μLEDs on the
707 implanted silicon probe. During water restriction, her health was monitored and she was
708 weighed daily to ensure she maintained at least 80% of her pre-restriction weight. Following

20

709 completion of these recordings, the second rat was kept on water restriction while she
710 performed the experiments outlined below in the "Behavioral Paradigm" section under
711 administration of saline or anisomycin. All procedures were performed in compliance with the
712 guidelines of the University of Michigan Animal Care and Use Committee.

Method details

714

Viral Constructs

716 For mice experiments we used an AAV9.*Syn*.GcaMP6f.WPRE.SV40 virus from the University of
717 Pennsylvania Vector Core/Addgene with an initial titer of ~4×10^{12} GC/mL and diluted it into
718 sterilized potassium phosphate buffered saline (KPBS) to a final titer of ~$2\text{-}4\times10^{12}$ GC/mL for
719 injection.

720 For rat experiments, we used an pGP.AAV9.*Syn*.GcaMP7f.WPRE.SV40 virus from the
721 University of Pennsylvania Vector Core/Addgene with an initial titer of 2.6×10^{13} GC/mL and
722 diluted it into sterilized phosphate buffered saline (PBS) to a final titer of 2.6×10^{12} GC/mL for
723 injection. Due to poor expression no imaging was performed.

Stereotactic Surgery

725 We performed two stereotactic surgeries and one base-plate implant on naïve mice, aged 3-8
726 months, according to previously published procedures (Kinsky et al., 2018; Resendez et al.,
727 2016). Both surgeries were performed under 1-2% isoflurane mixed with oxygen. Mice were
728 given 0.05mL/kg buprenorphine (Buprenex) for analgesia (subcutaneously, SC), 5.0mL/kg of
729 the anti-inflammatory drug Rimadyl (Pfizer, SC), and 400mL/kg of the antibiotic Cefazolin
730 (Pfizer, SC) immediately after induction. They were carefully monitored to ensure they never
731 dropped below 80% of their pre-operative weight during convalescence and received the same
732 dosage of Buprenex, Cefazolin, and Rimadyl twice daily for three days following surgery. In the
733 first surgery, a small craniotomy was performed at AP -2.0, ML +1.5 (right) and 250nL of
734 GcaMP6f virus (at the titer noted below) was injected 1.5mm below the brain surface at
735 40nL/min using a 1µL Hamilton syringe and infusion pump. The needle remained in place a
736 minimum of 10 minutes after the infusion finished at which point it was slowly removed, the
737 mouse's scalp was sutured, and the mouse was removed from anesthesia and allowed to
738 recover.

739 3-4 weeks after viral infusion, mice underwent second surgery to attach a gradient index (GRIN)
740 lens (GRINtech, 1mm x 4mm). After performing an ~2mm craniotomy around the implant area,
741 we carefully aspirated cortex using blunted 25ga and 27ga needles under constant irrigation
742 with cold, sterile saline until we visually identified the medial-lateral striations of the corpus
743 callosum. We carefully removed these striations using a blunted 31ga needle while leaving the
744 underlying anterior-posterior striations intact, after which we applied gelfoam for 5-10 minutes to
745 stop any bleeding. We then lowered the GRIN lens to 1.1mm below bregma. Note that this
746 entailed pushing down ~50-300µm to counteract brain swelling during surgery. We then applied
747 Kwik-Sil (World Precision Instruments) to provide a seal between skull and GRIN lens and then
748 cemented the GRIN lens in place with Metabond (Parkell), covered it in a layer of Kwik-Cast
749 (World Precision Instruments), and then removed the animal from anesthesia and allowed him

750 to recover after removing any sharp edges remaining from dried Metabond with a dental drill
751 and providing any necessary sutures.

752   Finally, after ~2-4 weeks we performed a procedure in which the mouse was put under
753 light anesthesia to attach a base plate for easy future attachment of a miniature epifluorescence
754 microscope (Ghosh et al., 2011, Inscopix, Inc.). Importantly, no tissue was cut during this
755 procedure. After induction, we attached the base plate to the camera via a set screw, set the
756 camera's focus level at ~1/3 from the bottom of its range, and carefully lowered the camera
757 objective and aligned it to the GRIN lens by eye, and visualized fluorescence via nVistaHD until
758 we observed clear vasculature and putative cell bodies expressing GcaMP6f (Resendez et al.,
759 2016). To counteract downward shrinking during curing, we then raised the camera up ~50μm
760 before applying Flow-It ALC Flowable Composite (Pentron) between the underside of the
761 baseplate and the cured Metabond on the mouse's skull. After light curing, we applied opaque
762 Metabond over the Flow-It ALC epoxy to the sides of the baseplate to provide additional
763 strength and to block ambient light infiltration. Mice were allowed to recover for several days
764 prior to habituation to camera attachment and performance of the behavioral task outlined
765 below. In the event that we did not observe clear vasculature and cell bodies when we first
766 visualized fluorescence we covered the GRIN lens with Kwik-Cast and removed the mouse from
767 anesthesia without attaching the baseplate. We then waited an additional week and repeated
768 the steps above.

769 For rats, we performed two surgeries in a similar manner as described above for mice.
770 However, rats were administered pre-operative and post-operative Meloxicam orally for
771 analgesia (in lieu of Buprenex) and triple-antibiotic was applied locally (in lieu of Cefazolin
772 injections) to the incision at the end of surgery. Meloxicam was additionally administered for two
773 days post-surgery during recovery, and animals were monitored daily for a minimum of seven
774 days during recovery. 0.4mL of a lidocaine/bupivacaine cocktail were given under the scalp to
775 provide local anesthesia at the incision site. In the first surgery, 1000nL of GCaMP7f virus was
776 infused in the prelimbic cortex at the center of a 1mm craniotomy (AP + 2.9, ML + 3.6, from
777 Bregma, DV -3.0 at an 18 degree angle from top of brain). Following infusion, ~1.5 mm of
778 overlying cortex was removed and a 23ga needle was lowered to ~500μm above the target site.
779 Then, a 0.6 x 7 mm GRIN lens was lowered to 3.0mm below the top of the brain, the area
780 between the skull and lens was sealed with Kwik-Sil, and the lens was affixed to the skull with
781 Vivid-Flow light-curable composite (Pearson Dental) and Metabond (Parkell). The lens was then
782 covered in Kwik-Sil for protection. During this surgery, ground and reference screws were also
783 placed over the cerebellum and a 3d printed crown base was attached to the rat's skull
784 (Vöröslakos et al., 2021) to which crown walls and top were connected and to further protect the
785 lens and future microdrive/probe implant. The rat was screened for fluorescence 8-12 weeks
786 later, but no cell dynamics were observed so no imaging equipment was implanted for this rat.

787 16 weeks later, the rat was again given pre-operative Meloxicam and anesthetized under
788 isoflurane for probe implant (Kinsky et al., 2023). The crown walls were removed and a 1.0mm
789 craniotomy was performed at AP-4.8, ML+3.6 from bregma. After removing dura and stopping
790 bleeding with cold, sterile saline, a NeuroNexus A1x32-5mm-50-177 probe, attached to a metal
791 microdrive, was implanted at 2.3 mm below the brain surface and the metal drive base was
792 attached to the skull with Unifast light cured dental epoxy (Henry-Schein). The craniotomy was
793 sealed with Dow-Sil, the probe was protected with dental wax, and the ground and reference
794 wires were connected to the probe electronic interface board (EIB). The crown walls were re-

22

795   attached, the EIB was connected to the crown walls, and the rat was removed from isoflurane
796   and allowed to recovery. The rat was monitored daily for 7 days prior to recording, during which
797   the probe was lowered ~1mm until sharp wave ripples and spiking activity were visualized
798   indicating localization of the probe in the CA1 cell layer. Full details including videos
799   demonstrating the implant process are also documented in Kinsky et al., (2023).

Histology procedures

801   Hippocampal slices were prepared following extraction from mice in accordance with the
802   standard methods and guidelines of the Boston University Animal Care and Use Committee. In
803   brief, mice were euthanized with Euthasol (Virbac), transcardially perfused with
804   paraformaldehyde (PFA), and decapitated. Following extraction, brains were placed in PFA for
805   approximately 48 hours before undergoing sectioning. Brains that were sliced using a Cryostat
806   underwent an additional step of sucrose cryoprotection and subsequent freezing in -80C. Brains
807   were mounted to the slicing platform using Tissue Tek O. C. T. (Sakura) and kept at -30C
808   throughout sectioning. 50μm slices were collected across the entire aspiration site in the dorsal
809   hippocampus region. Brains that were sliced using a vibratome were stabilized using super glue
810   and submerged in 1% PBS. A Leica VT1000 S vibratome was equipped with a platinum coated
811   double edged blade (Electron Microscopy Sciences , Cat. #72003-01) and set to a maximal
812   speed of 0.9mm/s for collecting 50 μm slices. Slices prepared from both the cryostat and
813   microtome were directly mounted onto (type of slides go here) and cover-slipped using DAPI
814   following sectioning. No histology was performed in the rat study.

815   For cell death (apoptosis) experiments, adult male mice weighing 20.1-25g were injected with
816   either anisomycin (150mg/kg, IP, ~0.11mL) or saline (IP, ~0.11mL) and perfused 4hr later with
817   PBS followed by 4% paraformaldehyde. Brain tissue was removed and fixed for 48hr in PFA.
818   Fixed tissue was sliced into 50μm thick free-floating sections and stored into 0.01% azide.
819   Tissue was sliced coronally (50um thickness) on a vibratome and stained using Biosensis
820   (Ready-to-Dilute) Fluoro-Jade C (FJC) staining kit. Hippocampal sections were selected and
821   mounted on charged slides and left to dry overnight for proper adhesion. Following kit
822   instructions, slides incubated in a coplin jar with 9 parts of 80% ethanol and 1 part of sodium
823   hydroxide for 5 minutes. Slides were then rinsed in 70% ethanol for 2 minutes followed by 2
824   minutes in distilled water. To minimize background fluorescence, slides were submerged in 9
825   part distilled water and 1 part potassium permanganate for 5 minutes, followed by 2 x 2 minute
826   rinses in distilled water. Slides were then incubated in 9 parts distilled water and 1 part FJC in
827   the dark for 15 minutes, followed by 3 x 1 minute rinses in distilled water. Finally, tissue dried for
828   10-20 minutes before being submerged in xylene for 10 minutes and mounted with DPX.
829   Fluorescence was visualized using a confocal microscope.

Behavioral Paradigm

831   Prior to surgery mice were handled to habituate them subsequent camera attachment. 3-7 days
832   following base plate attachment surgery we conditioned mice to the imaging procedures by
833   further handling them for 5-10 minutes for a minimum three days. During this handling a plastic
834   "dummy" microscope (Inscopix) of approximately the same size/weight as the imaging camera
835   was attached to each mouse's head and remained on his head for 1-2 hours in his home cage.
836   When it became easy to attach the scope to the mouse's head a real imaging miniscope was
837   attached to head and an optimal focus plane chosen. We then recorded three 5 minute imaging
838   videos at this focus and +/- ¼ turn (~25μm) in the mouse's home cage. These movies were

839   processed as described in the Image Acquisition and Processing section and an optimal zoom
840   was chosen based on whichever focus plane maximized cell yield and produced clear looking
841   cell bodies. Animals were then placed in a novel environment with a different size and shape
842   compared to the experimental environments for a 10 minute session to habituation them to the
843   general experimental outline and ensure that they explored novel arenas.

844   Following habituation to the imaging procedures mice performed a contextual fear
845   conditioning (CFC) task with simultaneous imaging of hippocampus neurons over the course of
846   10 days. Note that all recording sessions are referred to by their time relative to applying the
847   mild foot-shock and the arena in which the recording occurred: e.g., Shock Day -2 occurred in
848   the shock arena two days prior to foot-shock while Neutral 4 hours occurred four hours after
849   foot-shock in the neutral arena. A typical day (Days -2, -1, 1, 2, and 7) consisted of two separate
850   10 minute recording blocks/sessions: one in the Neural arena and one in the shock arena. Mice
851   first explored a square (neutral) arena, placed in the center of a well-lit room, for 10 minutes.
852   The neutral arena was a square constructed of 3/8" plywood (25cm x 25cm x 15 cm), which was
853   painted yellow with sealable paint. Additionally, one wall was painted with black horizontal
854   stripes for visual orientation purposes. The neutral arena was wiped down with 70% ethanol ~10
855   minutes prior to recording. After 10 minutes of exploration the experimenter took the mouse out
856   of the arena, leaving the miniscope camera on their head and placed the mouse in its home
857   cage on a moveable cart upon which it was immediately transported down a short hallway to
858   second room. Therefore, the time between the end of the neutral and shock arena recordings
859   was approximately five minutes.

860   The second room was dimly lit and contained the fear conditioning (shock) arena. The
861   shock arena (Coulbourn Instruments, Whitehall, PA, USA) consisted of metal-panel side walls,
862   Plexiglas front and rear walls, and a stainless-steel grid floor composed of 16 grid bars (22cm x
863   22cm). Following 10 minutes of exploration of the shock arena, mice were removed from the
864   arena, the camera was removed, and mice were returned to their home cage. Both arenas were
865   wiped down with 70% ethanol ~10min prior to recording to eliminate any odor cues. Note that
866   mice always explored the neutral arena first and the shock arena second. For the Day 0
867   sessions, mice first explored the neutral arena for 10 minutes and were transported to the shock
868   arena as usual. However, during this session (Shock Day 0) the mouse was immediately given
869   a single 0.25mA shock and allowed to explore the arena for an additional 60 seconds only
870   before being removed and returned to his cage. Efficacy of shock was confirmed post-hoc by
871   eye by the presence of jumping/darting behavior immediately post-shock. The 4 hour session
872   was identical to the Day -2, 1, 1, 2, and 7 sessions. With the exception of the 4 hour session, all
873   recording sessions were performed in the first half of the mouse's life cycle while the 4 hour
874   session occurred in the second half of the light cycle.

875   On day zero, after the camera was removed and prior to returning to their home cage, mice
876   received an intraperitoneal injection of either anisomycin (150 mg/kg, Sigma-Aldrich A9789) or
877   the equivalent amount of vehicle. After injection, they were returned to their cage for 4 hours
878   until the next recording session began.

879   Following extensive habituation to a rest box during the seven day recovery period, rat neural
880   activity and behavior was recorded across ~ 5 hours. Following a 15-30 minute baseline
881   recording (PRE) in the rest box, the animal was given an I.P. injection of anisomycin and then
882   immediately placed on a novel linear track which he explored for 45 minutes (TRACK). The rat
883   was then placed back into the rest box for 3.5 hours (POST). Following that, the animal was

884 placed on a second novel track for 45 minutes (TRACK2) followed by a brief recording in the
885 rest box (POST2). The second rat underwent a similar procedure, except that there was a 2
886 hour POST recording prior to the TRACK recording and no POST2 recording. Similar
887 procedures were followed the day before and after anisomycin injection but using saline for
888 injection instead of anisomycin. Data was acquired continuously throughout with the exceptions
889 of periodic cable disconnections to perform the I.P. injection, start a new recording epoch, and
890 disconnect/reconnect cables that became twisted.

891 **Anisomycin**

892 For mice recordings, 25 mg of anisomycin (Sigma Aldrich) was dissolved into 50 µL of 6N HCl
893 and 500 µL of 1.8%NaCl. ~125 µL of 1N NaOH was then added to the solution followed by 0.1-
894 0.5 µL of 1N NaOH, testing pH after each addition until a final pH of 7.0 to 7.5 was reached, with
895 a final concentration of 24-27 mg/mL. In the case that pH rose above 7.5 during titration and
896 and/or the anisomycin went back into precipitate, small amounts (10-20 µL) of 6N HCl were
897 added until particles were no longer visible and the titration with 1N NaOH was restarted. Mice
898 were administered 150mg/kg of anisomycin solution via intraperitoneal injection, or ~0.15-
899 0.18mL for a typical 30g mouse.

900 For rat recordings, 100mg of anisomycin was dissolved into 1.6mL of 0.1N HCl (in 0.9% saline).
901 ~240 µL of 1N HCl was added, then 10-12 µL of NaOH was added in 1-2 µL amounts, testing
902 pH between each step until a pH of 7-7.5 was reached. 0.9% Saline was then added until the
903 appropriate concentration was reached to inject 1.5mL of anisomycin at 150mg/kg. In one rat
904 (Rat1 in Figure S5), due to a small amount of waste, the final amount injected corresponded to
905 100 mg/kg.

Quantification and statistical analysis

907

Behavioral Tracking and Fear Metrics

909 We utilized two different camera/software configurations for tracking animal behavior. Both
910 configurations generated a TTL pulse at the beginning of behavioral tracking to synchronize with
911 image acquisition. We utilized Cineplex software (v2, Plexon) to track animal location at 30Hz in
912 the neutral arena. We used FreezeFrame (Actimetrics) to track animal location in the shock
913 arena at 3.75Hz. Animal location was obtained post-hoc via custom-written, freely available
914 Python software (www.github.com/wmau/FearReinstatement). We observed inconsistent frame
915 rates and inaccurate acquisition of behavioral video frames for one mouse in the neutral arena
916 during the day 0, 4 hour, and day 1-2 sessions. These sessions were excluded from analysis.

917 Freezing was calculated by first downsampling neutral position data to 3.75 Hz to match the
918 sample rate used in the shock arena. We then identified freezing epochs as any periods of 10
919 consecutive frames (2.67 seconds) or more where the mouse's velocity was less than
920 1.5cm/second.

Neural Discrimination

922 We evaluated the extent to which each animal's behavior reflected the expression of a context-
923 specific fear memory through a behavioral discrimination index (DI_{beh}), calculated as follows:

25

924
$$DI_{beh} = \frac{Frz_{Neutral} - Frz_{Shock}}{Frz_{Neutral} + Frz_{Shock}}$$

925 Where $Frz_{Neutral}$ and Frz_{Shock} are the percentages of time spent freezing in the neutral and shock
926 arenas, respectively. Thus, a negative DI_{beh} value indicated more freezing behavior in the shock
927 arena (indicating successful encoding of a context-specific fear memory), a positive DI_{beh} value
928 indicated more freezing behavior in the neutral arena, and a DI_{beh} value around zero indicated
929 equal/low freezing behavior in each arena (indicating the formation of a non-specific or weak
930 fear memory).

931 **Imaging Acquisition and Processing**

932 Brain imaging data was obtained using nVista HD (Inscopix) at 720 x 540 pixels and a 20 Hz
933 sample rate. Note that imaging data for one mouse was obtained at 10 Hz. Prior to
934 neuron/calcium event identification we first pre-processed each movie using Inscopix Imaging
935 Suite (Inscopix) software. Preprocessing entailed three steps a) motion corrections, and b)
936 cropping the motion-corrected movie to eliminate any dead pixels or areas with no calcium
937 activity, and c) extracting a minimum projection of the pre-processed movie for later neuron
938 registration. We did not analyze one imaging session in which we had to reconnect the camera
939 cable mid-session and could not synchronize the imaging data with behavioral data. Maximum
940 projections of imaging movies were made using the Inscopix Imaging Suite or custom-written
941 functions based off of an open-source MATLAB library (Muir & Kampa, 2015).

942 **Electrophysiological Recordings**

943 Data was acquired using an Intan 1028 channel recording system through OpenEphys software
944 into binary format and behavior was tracked using Optitrack high resolution cameras and Motive
945 image acquisition software.

946 **Data Analysis**

947 Data analysis was performed in both Python and MATLAB software. Python analysis code is
948 available at https://github.com/nkinsky/Eraser.

949 **Spike sorting and analysis**

950 Electrophysiological recordings were automatically clustered using SpyKING CIRCUS software
951 (Yger et al., 2018) and units were manually curated in phy (https://github.com/cortex-lab/phy/).
952 Units were grouped into single units if they exhibited a clear refractory period and were well-
953 isolated from other putative spikes. Other units which exhibited a clear waveform but were either
954 poorly isolated or exhibited refractory period violations were classified as multi-unit activity
955 (MUA). All single units and MUA were combined and cross-correlograms for the combined
956 activity were created for each epoch of the recording separately.

957 **Tenaspis**

958 Neuron regions-of-interest (ROIs) and calcium events were identified using a custom written,
959 open source algorithm employed in MATLAB 2016b called A Technique for Extracting Neuronal
960 Activity from Single Photon Neuronal Image Sequences (Tenaspis) (Mau et al., 2018). This
961 procedure was comprehensively documented in Kinsky et al., 2018:

962 "Tenaspis is open-source and available at: https://github.com/SharpWave/TENASPIS. First,
963 Tenaspis filters each calcium imaging movie with a band-pass filter per (Kitamura et al., 2015)
964 to accentuate the separation between overlapping calcium events. Specifically, Tenaspis
965 smooths the movie with a 4.5 μm disk filter and divides it by another movie smoothed with a
966 23.6 μm disk filter. Second, it adaptively thresholds each imaging frame to identify separable
967 pockets of calcium activity, designated as blobs, on each frame. Blobs of activity are accepted
968 at this stage of processing only if they approximate the size and shape of a mouse hippocampal
969 neuron, as measured by their radius (min = ~6μm, max = ~11μm), the ratio of long to short axes
970 (max = 2), and solidity (min = 0.95), a metric used by the *regionprops* function of MATLAB we
971 employ to exclude jagged/strange shaped blobs. Third, Tenaspis strings together blobs on
972 successive frames to identify potential calcium transients and their spatial activity patterns.
973 Fourth, Tenaspis searches for any transients that could results from staggered activity of two
974 neighboring neurons. It rejects any transients whose centroid travels more than 2.5μm between
975 frames and whose duration is less than 0.20 seconds. Fifth, Tenaspis identifies the probable
976 spatial origin of each transient by constructing putative regions-of-interest (ROIs), defined as all
977 connected pixels that are active on at least 50% of the frames in the transient. Sixth, Tenaspis
978 creates initial neuron ROIs by merging putative transient ROIs that are discontinuous in time but
979 occur in the same location. Specifically, it first attempts to merge all ROIs whose centroids are
980 less than a distance threshold of ~0.6μm from each other. In order to merge two transient ROIs,
981 the two-dimensional Spearman correlation between the ROIs must yield $r^2 > 0.2$ and $p < 0.01$.
982 Tenaspis then successively increases the distance threshold and again attempts to merge ROIs
983 until no more valid merges occur (at a distance threshold of ~3μm, typically). Seventh, Tenaspis
984 integrates the fluorescence value of each neuron ROI identified in the previous step across all
985 frames to get that neuron's calcium trace, and then identifies putative spiking epochs for each
986 neuron. Specifically, it first identifies the rising epochs of any transients identified in earlier
987 steps. Then, it attempts to identify any missed transients as regions of the calcium trace that
988 have a) a minimum peak amplitude > 1/3 of the transients identified in step 3, b) a high
989 correlation ($p < 0.00001$) between active pixels and the pixels of the average neuron ROI
990 identified in step 6, and b) a positive slope lasting at least 0.2 seconds. Last, Tenaspis searches
991 for any neuron ROIs that overlap more than 50% and whose calcium traces are similar and
992 merges their traces and ROIs."

993 **Between Session Neuron Registration**

994 We utilized custom-written, freely available MATLAB code (available at
995 https://github.com/nkinsky/ImageCamp) to perform neuron registration across sessions in
996 accordance with previous results (Kinsky et al., 2018). The details of this procedure described in
997 Kinsky et al. (2018) are reproduced here:

998 "Neuron registration occurred in two steps: session registration and neuron registration.

999 *Session registration* – Prior to mapping neurons between sessions, we determined how
1000 much the imaging window shifted between sessions. In order to isolate consistent features of
1001 the imaging plane for each mouse (such as vasculature or coagulated blood), we created a
1002 minimum projection of all of the frames of the motion-corrected and cropped brain imaging
1003 movie for each recording session. One session ("registered session") was then registered to a
1004 base session using the "imregtform" function from the MATLAB Image Processing Toolbox,
1005 assuming a rigid geometric transform (rotation and translation only) between images, and the
1006 calculated transformation object was saved for future use.

1007   *Neuron Registration* – Next, each ROI in the registered session was transformed to its
1008   corresponding location in the base session. Each neuron in the base session was then mapped
1009   to the neuron with the closest center-of-mass in the registered session, unless the closest
1010   neuron exceeded our maximum distance threshold of 3 pixels (3.3 µm). In this case the base
1011   session neuron was designated to map to no other neurons in the registered session. If, due to
1012   high density of neurons in a given area, we found that multiple neurons from the base session
1013   mapped to the same neuron in the registered session, we then calculated the spatial correlation
1014   (Spearman) between each pair of ROIs and designated the base session ROI with the highest
1015   correlation as mapping to the registered session ROI.

1016   For multiple session registrations, the same procedure as above was performed for each
1017   session in two different ways. First, we registered each session directly to the first session in the
1018   experiment and updated ROI locations/added new ROIs to set of existing ROIs with each
1019   registration. This helped account for slight day-to-day drift in neurons ROIs due to shifts in
1020   vasculature, build-up of fluid underneath the viewing window, creep/shrinkage of dental cement,
1021   etc. Second, to ensure that neuron ROIs did not drift excessively across sessions we also
1022   performed all the above steps but did NOT update ROI locations allowing us to register each set
1023   of ROIs to those furthest away chronologically. The resulting mappings were then compared
1024   across all sessions, and any neuron mappings that differed between the two methods (e.g.,
1025   ROIs that moved excessively across the duration of the experiment) were excluded from
1026   analysis. Those that remained in the same location were included."

1027   The procedure to assess the quality of across session registration was described in
1028   Kinsky et al. (2018) and is reproduced here: "We checked the quality of neuron registration
1029   between each session-pair in two ways: 1) by plotting the distribution of changes in ROI
1030   orientations between session and comparing it to chance, calculated by shuffling neuron identity
1031   between session 1000 times, and 2) plotting ROIs of all neurons between two sessions and
1032   looking for systematic shifts in neuron ROIs that could lead to false negatives/positives in the
1033   registration." All session-pairs (except those few in which we could not synchronized imaging
1034   and behavioral data as noted above) met the above two criteria and were thus included in our
1035   analysis.

1036   Cells that had calcium activity in the first session (neutral arena) for which we did not identify a
1037   matching neuron in the second session (shock arena) were classified as OFF cells. Likewise,
1038   neurons active in the shock arena with no matching partner in the neutral arena were classified
1039   as ON cells.

1040   All neuron registrations were cross validated by overlaying ROIs from each session and
1041   evaluating their match by eye. In a few cases, we noticed erroneous registrations and adjusted
1042   our between-session neuron alignment by calculating the rigid geometric transformation using
1043   4-5 cell ROIs active in both sessions. Figure S11 provides examples of our between-session
1044   neuron registration results and quantification procedures.

1045   **Neural Discrimination Metrics**

1046   The extent to which gross hippocampal ensemble activity differed between arenas was
1047   calculated in two ways. First, we calculated the proportion of cells that turned ON and OFF
1048   between arenas divided by the total number of cells active in either arena.

1049 Next, we calculated the extent to which each neuron active in both arenas distinguished
1050 between arenas by changing its event rate in a manner analogous to $DI_{beh.}$ However, we took
1051 the absolute value to account for the fact that both positive and negative event rate changes
1052 could reflect neural differentiation between arenas. Then, we took the mean across all neurons
1053 to obtain a neural discrimination index (DI_{Neuron}):

$$1054 \qquad DI_{Neuron} = \left| \frac{ER_{Neutral} - ER_{Shock}}{ERz_{Neutral} + ER_{Shock}} \right|$$

1055

1056 Generalized Linear Model (GLM) to Assess anisomycin effects on the number of active
1057 cells

1058 All GLM analyses were performed using the *GLM* function in the Python *statsmodels* package.
1059 The dependent variable was the number of neurons recorded in each session, normalized to the
1060 amount recorded on Day -2. Covariates included were a constant/intercept term, group (ANI
1061 vs. CTRL), arena (Shock vs. Neutral), anisomycin stage (acute = 4 hour, after = Days 1, 2, and
1062 7), freezing ratio, and two interaction terms: group x acute and group x after. The GLM was fit
1063 assuming a gaussian distribution with the identify link function and using the iteratively
1064 reweighted least squares method.

1065 Placefield Analysis

1066 Calcium transients occurring when the mouse was running greater than or equal to
1067 1.5cm/second were spatially binned (1cm by 1cm) and occupancy normalized following which
1068 place fields were identified and quantified in a manner similar to Kinsky et al. (2018),
1069 reproduced here:

1070 "Spatial mutual information (SI) was computed from the following equations, adapted from
1071 (Olypher et al., 2003)

$$1072 \qquad I_{pos}(x_i) = \sum_{k=0}^{1} P_{k|x_i} \, log \left(\frac{P_{k|x_i}}{P_k} \right)$$

$$1073 \qquad SI = \sum_{i=1} P_{x_i} I_{pos}(x_i)$$

1074 where:

1075   - P_{x_i} is the probability the mouse is in pixel x_i

1076   - P_k is the probability of observing k calcium events (0 or 1)

1077   - $P_{k|x_i}$ is the conditional probability of observing k calcium events in pixel x_i.

1078 The SI was then calculated 1000 times using shuffled calcium event timestamps, and a neuron
1079 was classified as a place cell if it 1) had at least 5 calcium transients during the session, and 2)
1080 the neuron's SI exceeded 95% of the shuffled Sis…We defined the extent of a place field as all
1081 connected occupancy bins whose smoothed event rate exceeded 50% of the peak event rate
1082 occupancy bin."

1083   Since spatial mutual information is biased by the number of samples (Olypher et al., 2003), we
1084   re-sampled the behavioral tracking data to match that of the imaging data (20Hz). This required
1085   up-sampling the shock arena data (3.75Hz->20Hz) and down sampling the neutral arena data
1086   (30Hz->20Hz).

1087   Placefield similarity between sessions was assessed by first smoothing the 2-d occupancy
1088   normalized event rate maps with a gaussian kernel (2.5cm std), flattening the smoothed maps
1089   into a vector, and then performing a Spearman correlation between all neurons active in both
1090   sessions. To quantify chance-level place field similarity we randomly shuffled the mapping
1091   between neurons from the first to the second session before performing the Spearman
1092   correlation. We then repeated this procedure 100 times.

1093   To assess the possibility that the configuration of place fields rotated together coherently
1094   between sessions (Kinsky et al., 2018), we again performed a Spearman correlation but after
1095   rotating the 2-d occupancy map in the second session 90 degrees. Since, due to small camera
1096   distortions, some 2-d occupancy maps were not square, one some occasions we resized
1097   (minimally) the second map to match the size/shape of the first map using the reshape function
1098   in Python's *numpy* package prior to correlate the two maps. We repeated this in successive 90
1099   degree increments and then took the mean correlation of all neurons that were active in both
1100   sessions to determine the optimal/"best" rotation of the place field map as that which maximized
1101   the correlation between sessions.

1102   We also performed a "center-out" rotation analysis to assess coherent place field rotations
1103   between sessions. First, the angle to the pixel with the maximum occupancy normalized event
1104   rate was identified for each cell. Second, this angle was recalculated for the same cell in a
1105   different session in the same box. These two angles were subtracted to get the "center-out"
1106   rotation between sessions. Sessions which exhibited a coherent rotation displayed a peak in a
1107   histogram of center-out angles at 0, 90, 180, or 270 degrees, while sessions which exhibited
1108   global remapping exhibited a uniform distribution of rotation angles.

1109   **Freeze-predicting Cell Analysis**

1110   Freeze onset and offset times were first identified for each mouse/session as noted in the
1111   *Behavioral Tracking and Fear Metrics* section above. We then formed calcium event rasters
1112   using the neural activity for each cell +/- 4 seconds from freeze onset, organizing the data into a
1113   *nfreeze_onsets x ntime_bins* array. We then summed this raster along the 0th dimension to get
1114   a freeze tuning curve. To calculated significance, we randomly, circularly shifted the putative
1115   spiking activity for a cell and calculated a shuffled tuning curve in a similar manner to the actual
1116   data. We repeated this procedure 1000 times, and calculated significance for each time bin as
1117   the number of shuffles where the shuffled tuning exceeded the actual tuning curve divided by
1118   1000. Last, we designated cells as significantly freeze-tuned if they had 3 or more bins with $p <$
1119   0.01 and were active on at least 25% of freezing events.

1120   **Covariance Analysis**

1121   Putative spiking activity for each cell was first binned into 0.5 second windows and z-scored
1122   after binning, forming a *ncells x nbins* array. The covariance of this array was then calculated
1123   using the *cov* function in numpy, returning a *ncells x ncells* array. For between-session
1124   comparisons, cells active in both sessions were registered and a new array was formed with the
1125   base (1st) session covariance in the lower diagonal and the registered (2nd) session in the upper

30

1126   diagonal. All entries along the main diagonal were ignored. This analysis was also performed
1127   including only peri-freeze times (to assess peri-freeze covariance), after randomly
1128   downsampling the number of freeze epochs to match the average from days -2 and -1 (to
1129   control for increased sampling on days 1 and 2), and after excluding all peri-freeze times (to
1130   assess non peri-freeze covariance).

Coactivation Analysis

1132   Putative spiking activity was first binned relative to the start of each freezing epoch ("freeze
1133   onset"), yielding a *nfreeze_onsets x nbins* array of binarized neural activity (1 = active, 0 =
1134   inactive). Pairwise coactivation was then calculated by taking the dot product of the binarized
1135   neural activity arrays between each pair of cells and taking the mean along the first axis,
1136   yielding the probability that both cells in a given cell-pair were active in each sampling bin. To
1137   calculate population-level coactivity, the number of active cells was first calculated for each
1138   recording session. The average number of active cells was then calculated across all peri-
1139   freeze trials (+/- 4 seconds) and this number was z-scored relative to activity across the entire
1140   session. To determine which cell-pairs exhibited significant pairwise coactivity beyond chance
1141   level, we first formed a *nfreeze_onsets x nbins* array of neural activity for each cell in a pair. We
1142   then randomly permuted the rows of the array for the second cell in the pair and calculated a
1143   shuffled level coactivation probability for that pair as described above. We repeated this process
1144   100 times for each cell pair, and then calculated a p-value for each bin as 1 – (# of bins where
1145   shuffle exceeds actual coactivity) / 100. A cell-pair was designated to have significant pairwise
1146   coactivation if it had > 3 consecutive bins with $p < 0.05$.

Hierarchical Bootstrapping

1148   We utilized hierarchical bootstrapping (HB, Saravanan et al., 2020) to estimate confidence
1149   intervals and P-values for different metrics in line with code found at
1150   https://github.com/soberlab/Hierarchical-Bootstrap-Paper. For each metric we generated a
1151   population of 10,000 values by resampling with replacement at each level of the data hierarchy
1152   (first mouse, then for each mouse, one session, then the variable measured, e.g. place field
1153   correlations or freeze-predicting cell covariance). We then pooled all the values and calculated
1154   the test statistic (typically the mean) and corresponding confidence interval / interquartile range.
1155   One or two-tailed tests were used with $\alpha = 0.05$, and the p-value was calculated by using the
1156   joint probability distribution of the bootstrapped samples to determine that the mean of one
1157   group was greater than the mean of the other group. All hierarchical bootstrapped data was
1158   visualized using boxplots (mean and 1st/3rd quartiles) with whiskers extending to the 95%
1159   confidence intervals created using the boxplot function from the Python package *Seaborn*.
1160   Chance level was calculated by shuffling cell identity before calculating each metric, and the
1161   mean and 95% confidence intervals were visualized using the *matplotlib* package.

Parametric statistics

1163   Where applicable, all parametric statistics used are noted in the corresponding figure legend.

1164

1165   FIGURE LEGENDS

1166   **Figure 1: Mice exhibit variability in memory recall and neural activity prior to learning in a**
1167   **contextual fear conditioning task . A)** Schematic of the behavioral paradigm. Mice freely explored two
1168   distinct arenas (neutral and shock) for 10 minutes each day. Mice underwent mild contextual fear
1169   conditioning on day 0 in the shock arena followed by immediate I.P. administration of anisomycin or
1170   vehicle in their home cage. Memory recall tests were conducted 4 hours and 1, 2, and 7 days post-shock.
1171   The time of each session is referenced to the shock session. **B)** (left) Learner (CTRL) mice freezing on all
1172   days. Red = shock arena, blue = neutral arena. *p=4.5e-0.4 shock – neutral freezing from day-1 to day 1
1173   one-sided paired t-test (n=4 mice, t=13.4). (right) Same but for Non-Learner (CTRL) mice (n=3 mice,
1174   p=0.249, t=0.819). **C)** Same as B but for ANI group (n=5 mice, p=0.219, t=0.859). **D)** Behavioral
1175   discrimination between arenas after shock (Days 1-2) shows formation of a specific fear memory for
1176   Learners only, by definition (positive = more freezing in neutral arena, negative = more freezing in shock
1177   arena, 0 = equal freezing in both arenas). *p=0.009 (t=3.56), #p=0.06 (t=1.83) 1-sided t-test of mean DI
1178   value from Days 1 & 2, n=8/6/10 sessions for Learners/Non-Learners/ANI group. **E)** (left) Neural overlap
1179   plots between neutral and shock arenas for an example Learner mouse on day -1, before shock. Green =
1180   cells active in the shock arena only, yellow = cells active in the neutral arena only, orange = cells active in
1181   both arenas. (right) Same for example Non-Learner on day -2 showing higher overlap of active cells
1182   between arenas. **F)** Example calcium activity from the Learner mouse shown in C (left) for cells active in
1183   both arenas. Black = calcium trace, red = putative spiking activity during transient rises. Top row shows
1184   shock arena preferring cells, bottom row shows neutral arena preferring cells. **G)** Neural discrimination
1185   index (DIneural) between groups on Days -2 and -1. Boxplots show population median and 1st/3rd
1186   quartiles (whiskers, 95% CI) estimated using hierarchical bootstrapping (HB) data with session means
1187   overlaid in dots, #p=0.09 after Bonferroni correction for multiple comparisons**. H)** Same as G) but for
1188   event rate in Shock arena**, I)** Same as G) but for event rate interquartile range (IQR) in Shock arena. **J)**
1189   Freezing in Neutral arena on Day 2 vs. Neutral arena on Day 0. Pearson correlation value and p-value
1190   (two-sided) shown on plot. Statistics for G-J: un-paired one-sided HB test for days -2 and -1 after
1191   Bonferroni correction, n=10,000 bootstraps.

1192   **Figure 2: Preventing protein synthesis accelerates cell turnover and stifles learning-related place**
1193   **field remapping. A)** Cell overlap ratio with Day -2 session, CTRL group. Blue = within shock arena, red =
1194   shock v. neutral arena. **B)** Same as A) but for ANI group. **C)** Change in overlap ratios from A) and B), dots
1195   show values from both arenas for each mouse, **p=0.00174 two-sided t-test of mean value for each
1196   mouse (t=4.11, n=7 CTRL mice and 5 ANI mice). **D)** Number of active neurons observed each day,
1197   normalized to day -1. p=2.e-5 freeze-ratio, #p=0.056 group x 4 hr session interaction, p=0.094 group x
1198   after interaction, generalized linear model. **E)** and **F)** Example place fields exhibiting learning-related
1199   remapping. **E)** Place field in shock arena from Learner mouse. (*top*) Example mouse trajectory (black)
1200   with calcium activity (red) overlaid for the same cell from day -2 to -1 in shock arena, *(bottom)* occupancy
1201   normalized rate maps for the same cells with warm colors indicating areas of high calcium activity. **F)**
1202   Same as E) but for Non-Learner mouse in Neutral arena. **G)** and **H)** Example stable place fields. **G)** Same
1203   as E) but for a different cell from same mouse in the shock arena prior to conditioning. **H)** Same as F) but
1204   for a different cell from the same mouse in the neutral arena after conditioning. **I)** Place field correlations
1205   for all mice before shock (Days -2 and -1), boxplots show population median and 1st/3rd quartiles
1206   (whiskers, 95% CI) estimated using hierarchical bootstrapping (HB) data with session means overlaid in
1207   dots. Dashed line and grey shading show mean and 95% CI of correlations calculated from shuffling cell
1208   identify 1000 times between sessions. **J)** Same as I) but for Day -1 to Day 1, *p=0.0496, **p=0.0034. **K)**
1209   Same as I) but for Day 1 to Day 2. **L)** Same as I) but for Day 2 to Day 7. Statistics for I-L: un-paired one-
1210   sided HB test after Bonferroni correction, n=10,000 bootstraps.

1211   **Figure 3: Arresting protein synthesis suppresses the development of coordinated freeze-**
1212   **predicting neural activity**. **A) and B)** Example traces from two freeze-predicting cells which exhibit
1213   coordinated activity prior to freezing event during the day 1 memory recall session in the shock arena.
1214   Red = putative spiking activity, pink = cell shown in C, blue = cell shown in E. **C)** After learning (Days 1
1215   and 2), z-scored population level calcium activity peaks between 0 and 2 seconds prior to freezing for
1216   CTRL relative to the ANI group. Line/shading = mean +/- 95% CI. Red: bins with p < 0.05, independent t-
1217   test (one-sided, n=7 CTRL mice and 5 ANI mice). **D) and E)** Example Learner freeze-predicting cells

32

1218   identified during the 4 hour (D) or day 1 (E) memory test tracked across sessions. Peri-event calcium
1219   activity rasters are centered on freeze onset time (solid green). Dashed green = baseline calcium event
1220   probability, red solid = peri-freeze calcium event probability, bins with p<0.01 (circular permutation test,
1221   n=1000) noted with red bars at top. D/E corresponds to pink/blue cells shown in A-B. Bold = session with
1222   significant freeze-tuning. **F)** Same as D and E but for ANI mouse freeze-predicting cell identified during
1223   the 4 hour session. **G)** Peri-freeze calcium event probability for all freeze-predicting cells detected for
1224   each group after learning (Days 1-2), sorted by time of peak activation. **H)** (left) Cumulative distribution of
1225   peak peri-freeze activation times before learning. *p=0.49, **p=1e-5 two-sided Wilcoxon rank-sum test , c:
1226   p=0.005 Non-Learners v. ANI, 1-sided Mann-Whitney U-test (n = 329/458/543 neurons for Learners/Non-
1227   Learners/ANI group) (right) same as left but for after learning. *p < 0.022, **p=2e-7 two-sided Wilcoxon
1228   rank-sum test. a: p=0.022 Learners v. Non-Learners, b: p=0.029 Learners v. ANI 1-sided Mann-Whitney
1229   U-test (n=194/315/366 neurons for Learners/Non-Learners/ANI group). **I)** Change in peak peri-freeze
1230   calcium event probability for all freeze-predicting cells detected during the Day 1 session and either the 4
1231   hour or Day 2 session. p < 0.02 1-way ANOVA each day separately, *p=0.02, **p=0.001, ***p=0.0006
1232   post-hoc Mann-Whiney U-test (n=30/35/29 4h to Day 1 cells and n = 35/37/45 Day 1 to Day 2 cells for
1233   Learners/Non-Learners/ANI group. **J)** Pairwise coactivation probability of all freeze-predicting cells for
1234   Learners during Before, 4 hour, and After sessions in Shock arena. Maroon/Black bars at top indicate
1235   significant increases in coactivation at 4 hour / After time points compared to before, p< 0.05 1-sided
1236   Mann-Whitney U-test (n= 4). **K)** Same as J) but for Non-Learners (n=3). **L)** Same as K) but for ANI group
1237   (n= 5). **M)** Same as K) but for Learners in Neutral Arena (n=4). **N)** Proportion of freeze-predictive cells
1238   with significant pairwise coactivation compared to chance (trial shuffle). *p=4e-8, **p=3.6e-7, #p=0.093.
1239   boxplots show population median and $1^{st}/3^{rd}$ quartiles (whiskers, 95% CI) estimated using hierarchical
1240   bootstrapping (HB) data with session means overlaid in dots. **O)** Freeze-predicting cells exhibit a trend
1241   toward increased peri-freeze covariance (z-scored relative to the Day -2 and -1 covariance values for all
1242   cells) for Learners but not Non-Learners or ANI group mice. Mean covariance of freeze-predictive cells
1243   from each session shown. #p=0.06. Statistics for K and O: un-paired one-sided HB test after Bonferroni
1244   correction, n=10,000 shuffles.

1245   **Figure S1**: **CTRL animals exhibit behavioral variability following learning and similar rates of cell**
1246   **turnover between arenas vs. across days.**

1247   **A)** CTRL mice freezing on all days. Red = shock arena, blue = neutral arena. **B)** Distribution of DI_{beh}
1248   scores for all mice in CTRL group on days 1 and 2. Dashed line indicates cutoff between Learners and
1249   Non-Learners. **C)** Cell overlap 1 day apart in the same arena (days -2 to -1 and 1 to 2) vs. cell overlap
1250   between arenas on the same day (days -2, -1, 1, 2) for all mice. *p=4.05e-7, ρ=0.81 Spearman
1251   correlation, n=26 overlap values across 13 mice. **D)** Same as C) but for neural discrimination index.
1252   *p=6.29e-7, ρ=0.82 Spearman correlation. **E)** Freeze ratio plots with each mouse's value connected by a
1253   line. **F)** No difference in thigmotaxis prior to conditioning in Neutral arena, dots show mean thigmotaxis
1254   ratio for each mouse from Days -2 and -1, p=0.23 ANOVA. **G)** Same as F) but in Shock arena, p=0.95
1255   ANOVA. **H)** Neutral arena freezing ratio for each session after shock plotted versus Neutral arena
1256   freezing on day of training (day 0) with Pearson correlation and associated p-value (two-sided) shown, n
1257   = 7 mice. **I)** Same as H) but for Shock arena freezing versus Neutral arena freezing on day of training.

1258   **Figure S2: Non-specific effects of Anisomycin include a reduction in locomotion**

1259   **A)** 4 mice were given I.P injections of anisomycin only (no shock) and their locomotion was tracked over
1260   24 hours. Normal activity did not return to baseline until between 6 and 24 hours later. Black solid/dashed
1261   lines = 4 hour mean +/- std freezing ratio for non-ANI fear conditioned mice shock arena (see B). **B)**
1262   Freezing ratios for all mice in the Shock arena prior to conditioning and 4 hours after conditioning shown
1263   for reference. **C)** Freezing ratios in Neutral arena immediately before and one day after conditioning.
1264   Lines show mean +/- std.

1265   **Figure S3: Absolute cell numbers recorded across all sessions**.

1266 **A)** Total number of neurons recorded across all sessions in Control group. **B)** Same as A but for ANI
1267 group. **C)** Same as A but for Learners. **D)** Same as A but for Non-Learners. **E)** Histogram of cell counts
1268 across all sessions with each group mean shown with dashed lines.

1269 **Figure S4: Anisomycin does not cause neuronal cell death at 4hr post injection in the**
1270 **hippocampus.**

1271 **A)** Experiment schematic. Animals were given I.P. injections of either ANI (n=8) or saline (n=7). 4 hours
1272 later, brains were extracted and processed for Fluoro-Jade C. **B)** Fluoro-Jade C positive neuronal count
1273 normalized to area; **C-H)** Representative images of whole hippocampus (HPC), CA1, and dentate gyrus
1274 (DG) in **C-E)** anisomycin-injected mice or **F-H)** saline- injected mice. Scale bar equals 200μm.

1275 **Figure S5: Reduced activity following anisomycin administration is not an imaging artifact and**
1276 **does not result from global disruption of electrical neural activity in hippocampal neurons.**

1277 **A-C)** Neural activity was tracked across ~5 hours before and after systemic administration of anisomycin
1278 in a rat. **A)** Cross correlograms for all single and multi-unit activity combined are shown from the pre
1279 epoch in a rest box (15 minutes), running on a novel track immediately following anisomycin injection (45
1280 minutes), post epoch in the rest box (3.5 hours), running on a second novel track (45 minutes), and a
1281 second post epoch in the rest box (15 minutes). Clear modulation of firing at the theta timescale is
1282 observed. **B)** Example trace from electrode in pyramidal cell layer of CA1 showing theta activity 10
1283 minutes and 4 hours 15 minutes post injection anisomycin injection. **C)** Example sharp wave ripple events
1284 occurring from 25 minutes to 4 hours 15 minutes post anisomycin injection across 9 channels of a linear
1285 probe spanning above to below the pyramidal cell layer. **D-F)** Same as A-C but for a different rat following
1286 systemic anisomycin injection. F) Shows one trace from an electrode in the cell layer with a raster of
1287 spiking activity from all units recorded shown below the trace, demonstrating a population burst coincident
1288 with each sharp wave ripple. **G-I)** Same as D-F but the following day after systemic saline (control)
1289 injection demonstrating no lasting effects of anisomycin 24 hours after injection. **J-K)** The signal-to-noise
1290 ratio of all mouse neurons captured using calcium imaging and active between sessions was tracked
1291 between sessions. **J)** Mean height of calcium transient peaks for all cells matched from day -1 to 4 hour
1292 session. p>0.63 both groups, two-sided t-test (n=8 CTRL and 7 ANI, 1 additional CTRL mouse included
1293 whose video tracking behavioral data was corrupted and could therefore could not be classified as a
1294 Learner or Non-Learner). **K)** Same as J) but tracking cells from day -1 to day 1, p>0.68 both groups, two-
1295 sided t-test.

1296 **Figure S6**: **Coherent Place Field Rotations Observed Between Sessions**

1297 **A)** Example animal trajectories from neutral arena day -2 (top row) and day -1 (middle row) with calcium
1298 activity overlaid (red). Each column corresponds to one cell. Bottom row shows data rotated 90 degrees,
1299 demonstrating a coherent rotation of spatial activity for all neurons. **B)** Smoothed, occupancy normalized
1300 calcium event maps corresponding to data shown in A). **C)** The angle from the center of the arena to
1301 each cell's maximum intensity place field center was calculated for each session (center-out angle).
1302 The distribution of center-out angles plotted, demonstrating a coherent rotation of place fields from Day -2
1303 to Day -1 by 90 degrees. **D)** Place field correlations (smoothed event maps) between sessions indicate
1304 apparently low stability across days without considering rotations, giving the false impression that the
1305 place field map randomly reorganizes between sessions. **E)** High correlations were observed after
1306 considering a coherent 90 degree rotation between sessions, indicating that place fields retain the same
1307 relative structure but rotate together as a whole. **F)** Mean correlations for each mouse without considering
1308 rotations gives the impression of instability before/after shock and heightened remapping for all groups
1309 from before to after learning. Boxplots show population median and $1^{st}/3^{rd}$ quartiles (whiskers, 95% CI)
1310 estimated using hierarchical bootstrapping (HB) data with session means overlaid in dots. Dashed line
1311 and grey shading show mean and 95% CI of correlations calculated from shuffling cell identify 1000 times
1312 between sessions.

1313 **Figure S7: Example stable and remapping place fields across sessions**

1314 **A)** Example place field plots for Learner mouse in Neutral arena Before conditioning (Day -2 to Day -1),
1315 from Before to After conditioning (Day -1 to Day 1), and After consolidation (Day 1 to Day 2)
1316 demonstrating high stability in Neutral arena across all time points. **(top row)** Mouse trajectory in black
1317 with cell calcium activity overlaid in red. **(bottom row)** Smoothed, occupancy normalized calcium event
1318 spatial maps corresponding to raw trajectory and event data shown in top row, with warmer colors
1319 indicating high event rates and cool colors indicating low event rates. Spearman correlation value
1320 between event rate maps shown at top. Dashed lines denote separate different cells at each time point,
1321 and solid lines separate different comparison times. **B)** Same as A) but for different Learner in Shock
1322 arena demonstrating remapping. Red box shows two example remapping cells in the Shock arena. **C)**
1323 and **D)** Same and A) and B) but for two different Non-Learners with red box showing remapping cells in
1324 the Neutral Arena. **E)** and **F)** Same as A) and B) but for two different ANI group mice showing stable
1325 place fields between sessions at all time points.

1326 **Figure S8: Place field correlations with STM (4 hour) session**

1327 **A)** Place field correlations for all mice combined for Day -1 vs 4 hour session. Boxplots show population
1328 median and 1st/3rd quartiles (whiskers, 95% CI) estimated using hierarchical bootstrapping (HB) data with
1329 session means overlaid in dots. Dashed line and grey shading show mean and 95% CI of correlations
1330 calculated from shuffling cell identity 1000 times between sessions. **B)** Same as A) but for 4 hour vs Day
1331 1 session. All hierarchical bootstrap test comparisons are ns. **C)** Place field correlations for all mice in
1332 each group from before to after shock (Day -1 to Day 1). Boxplots show population median and 1st/3rd
1333 quartiles (whiskers, 95% CI) estimated using hierarchical bootstrapping (HB) data with session means
1334 overlaid in dots. Significant p-values calculated using a one-sided HB permutation test are shown directly
1335 on each panel.

1336 **Figure S9: Population Vector (PV) correlations.**

1337 **A)-E)** 1D PV correlations between sessions including only cells active in BOTH sessions. **A)** Before (Day
1338 -2 vs -1), *p=0.042, ***p<0.0006. **B)** After (Day 1 vs 2) *p=0.034, #p=0.072. **C)** Before v After (Day -1 vs
1339 1), *p<0.039, **p=0.0098. **D)** Day -1 vs 4 hr session. **E)** 4 hr session vs Day 1 *p=0.0049, #p=0.076. **F)**
1340 Day 2 vs Day 7, *p=0.0189, **p=0.0164, #p=0.064. Green = Learners, Orange = Non-Learners, Blue =
1341 ANI. Boxplots show population median and 1st/3rd quartiles (whiskers, 95% CI) estimated using
1342 hierarchical bootstrapping (HB) data with session means overlaid in dots. Dashed line and grey shading
1343 show mean and 95% CI of correlations calculated from shuffling cell identify 1000 times between
1344 sessions. Statistics: un-paired one-sided HB test after Bonferroni correction.

1345 **Figure S10: Freeze-cell covariance increases are driven by Learners and not purely a result of less**
1346 **freezing in Non-Learners and the ANI group.**

1347 **A)-C)** Example freeze-predicting cells tracked across sessions forward and backward in time from the day
1348 indicated in bold. Peri-event calcium activity rasters are centered on freeze onset time (solid green).
1349 Dashed green = baseline calcium event probability, red solid = peri-freeze calcium event probability, bins
1350 with p<0.01 (circular permutation test) noted with red bars at top. D/E corresponds to pink/blue cells
1351 shown in A-B. **A)** Example freeze-predictive cell from Non-Learner **B)-C)** Example freeze-predicting cells
1352 from two different Learners. **D)** Proportion freeze-predicting cells detected in Neutral arena across days.
1353 Bars=mean, line=std. **E)** Same as D) but for Shock arena. **F)** After learning (Days 1 and 2), z-scored
1354 population level calcium activity peaks between 0 and 2 seconds prior to freezing for both Learners and
1355 Non-Learners. Line/shading = mean +/- 95% CI. Red: bins with p < 0.05, independent t-test (one-sided,
1356 n=4 Learners and 3 Non-Learners). **G)** Mean covariance of all cells in neutral arena prior to learning
1357 exhibit small changes, compare y-axis to Figure 3O and S10H, H.**p=0.0048, ***p<1e-8, #p=0.06. **H)**
1358 Same as G) but for all cells in shock arena. *p=0.026, **p=0.00052, ***p<2.5e-6. **I)** Same as G) but for
1359 freeze predictive cells only, peri-freeze times only, and after randomly downsampling the number of
1360 freeze events to match the average number observed during days -2 and -1. #p=0.056 **J)** Same as H) but
1361 excluding all peri-freeze times. *p=0.0018**p=1.2e-4, ***p=2.1e-5. **K)** Mean covariance of freeze-
1362 predicting cells detected on Day 1 tracked across time. #p=0.068. For G-K, boxplots show population
1363 median and 1st/3rd quartiles (whiskers, 95% CI) estimated using hierarchical bootstrapping (HB) data with

1364   session means overlaid in dots. Dashed line and grey shading show mean and 95% CI of correlations
1365   calculated from shuffling cell identify 1000 times between sessions. Statistics: un-paired one-sided HB
1366   test after Bonferroni correction. **L-M)** There are no significant differences between the proportion of active
1367   units (z-scored) peaks for Control animals compared to the ANI group between 0 and 2 seconds prior to
1368   freezing before conditioning (L) and at the 4 hour session (M). Line/shading = mean +/- 95% CI. Red: bins
1369   with $p < 0.05$, independent t-test (two-sided).

1370   **Figure S11: Between Session Neuron Registration Metrics**

1371   **A)** Example neuron registration between the Day -1 and 4 Hour session for one mouse in the shock
1372   arena depicting cell ROIs active during the Day -1 session only (blue), the 4 Hour session only (teal), and
1373   both the Day -1 and 4 Hour session (yellow) with ROIs which were successfully registered across
1374   sessions outlined in red. Insets show magnified ROIs and demonstrate that cells registered across days
1375   exhibit similar shape and orientation. **B)** and **C)** Minimum projections of the imaging movie from the
1376   sessions shown in A demonstrating high day-to-day stability, evidenced by clear alignment of landmarks
1377   (e.g. vasculature) between sessions. **D)** Change in ROI orientation for all neurons registered to the Day -2
1378   session for the mouse shown in A). Note that the majority of registered neurons exhibit very small
1379   changes in orientation between sessions, even up to 9 days later (Day -2 to Day 7). **E)** and **F)** Similar to
1380   D) but for all mice in the CTRL and ANI groups separately for Day -1 to Day 4 (from before to after
1381   anisomycin administration). Note a similar distribution of ROI orientation changes, indicating that the
1382   observed acceleration of cell turnover following anisomycin administration is not due to poor neuron
1383   registration. **G)** Side-by-side comparison of all neuron ROI changes for each group shown as a
1384   cumulative density function.